Addis Ababa University
Addis Ababa Institute of Technology
School of Electrical and Computer Engineering

Asphalt Pavement Thickness Estimation and Material Characterization

A Thesis submitted to
School of Electrical and Computer Engineering
Addis Ababa Institute of Technology

In Partial Fulfillment of the Requirements for the Degree of Master of Science (Communication Engineering)

By:
Tewodros Mulugeta
Adviser: Ephrem Teshale (PhD)
Co-Adviser: Mequanent Mulugeta (MSc)

Addis Ababa, Ethiopia
January 16, 2019

Declaration

I, the undersigned, declare that the thesis comprises my own work in compliance with internationally accepted practices; I have fully acknowledged and referred all materials used in this thesis work.

Tewodros Mulugeta

Name	Signature

Addis Ababa University
Addis Ababa Institute of Technology
School of Electrical and Computer Engineering

This is to certify that the thesis prepared by **Tewodros Mulugeta**, entitled *Asphalt Pavement Thickness Estimation and Material Characterization* and submitted in partial fulfillment of the requirements for the degree of Master of Science (Communication Engineering) complies with the regulations of the University and meets the accepted standards with respect to originality and quality.

Signed by the Examining Committee:

Internal Examiner	_____	Signature	_____	Date	_____
External Examiner	_____	Signature	_____	Date	_____
Adviser	Ephrem Teshale (PhD)	Signature	_____	Date	_____
Co-Adviser	Mequanent Mulugeta	Signature	_____	Date	_____

_____
Dean, School of Electrical and Computer Engineering

ABSTRACT

Asphalt pavement is one of the most dominant infrastructure consuming huge investment and play as a blood vessel to a nation. The surface layer of asphalt pavement is a multilayer structure. It commonly has three sub-layers: the top surface layer (Asphalt), the intermediate surface layer (Base course) and the following surface layer (Sub base). The thicknesses of the surface layer and the top surface layer have great importance on quality condition and maintenance of asphalt pavements.

Estimating asphalt pavement layer thicknesses and material type accurately helps to evaluate the pavement condition. Common methods of estimation of these parameters includes boring a hole (coring) at selected sampling points, used to estimate the asphalt layer thicknesses and material characterization, have limitations. Ground Penetrating Radar (GPR) represents an alternative non-destructive approach which alleviates some of this limitation.

GPR signal processing is a non-destructive technique, particularly promising for pavement characteristics interpretation. The accuracy of asphalt pavement layer thicknesses estimation and material characterization depends on GPR data analysis employing different estimation approaches and based on the incoming signal from the radar. The focus of the thesis is to investigate asphalt pavement thickness and material characterization using GPR data. Finite Difference Time Domain (FDTD) simulation and GPRmax are tools used to validate the research. This has to be taken seriously.

KEYWORDS

GPRMax, GPR, Matching Filter, Dielectric Constants, Asphalt Pavement Layer Thickness

ACKNOWLEDGMENTS

I owe my deepest gratitude to my advisor Ephrem Teshale (PhD) give me the opportunity to participate on this research work and for his guidance, encouragements, and support during this research. Special thanks are also given to my co-advisor Mequanent Mulugeta (MSc.) for his contribution in enhancing the quality of this research. They always been available and willing to help me. Besides God!

Special thanks are extended to the Ethiopian Construction Project Management Institute (ECPMI) for supporting the research.

My highest gratitude goes to all my family member for their love and encouragement. Without their love and support I would not have accomplished this work.

Finally, I would like to express my thanks and appreciation to all my friends from School of Civil Engineering (Road and Transport Master's Student) and my Classmates all the new friends I made during my work in Addis Ababa Institute of Technology (AAiT).

CONTENTS

LIST OF FIGURES

LIST OF TABLES

ACRONYMS

AAiT Addis Ababa Institute of Technology

ECPMI Ethiopian Construction Project Management Institute

E Electric Field

ESPRIT Estimation of signal parameter via rotation invariance techniques

FIR Finite Impulse Response

FDTD Finite Difference Time Domain

GPR Ground Penetrating Radar

GUI Graphical User Interface

H Magnetic Field

HPC High Performance Computing

IIR Infinite Impulse Response

MPI Messaging Passing Interface

NDT Non Destructive Techniques

MUSIC Multiple signal classification

VTK Visualization Tool Kit

1 INTRODUCTION

This chapter presents the basic application areas and types of non- destructive methods, research problem, goals and objectives, the significance of this research in Asphalt pavement structure. The literature that have been done by other scholars and researcher work is acknowledged. Finally, overall method and chapter organization of the thesis is presented.

In developing country like Ethiopia construction sector has a significant contribution on development and creating jobs areas for the nation. However, number of challenges are crippling and testing the strength of management systems of sector. Many investigations agreed on the poor construction management system of the sector which creates a corrupted and poor quality of construction. In addition, to the system drawback, the application of different technologies for quality control and inspection is very limited [1], [2]. Therefore, a sustainable construction industry is achieved when the sector is supported by the up to dated technology and advanced quality control mechanisms are in place.

For the last three decades Non Destructive Techniques (NDT) technology are becoming popular around the world [3]. There are different types of NDT tools and devices such as ground penetrating radar GPR, ultrasonic equipment, Percometer and other surface detection devices. The non-destructive testing technology have multiple advantages in terms data accuracy, time saving and post-processing of the data from the NDT machines to other decision-making procedures.

1.1 GROUND PENETRATING RADAR (GPR)

Ground Penetrating Radar is a safe, advanced, and non-invasive sensing techniques that has several tradition and novel applications. It can be effectively used for subsurface investigation, three- dimensional imaging of composite structures, and diagnostics affecting the whole life cycle of civil engineering works.[2]

Ground penetrating radar is now a well-accepted geophysical technique. The method uses radio waves to investigate "the ground" which means any low loss dielectric material. In its earliest inception, GPR was primarily applied to natural geologic materials. Now GPR is equally well applied to a host of other media such as wood, concrete, and asphalt.

GPR is a Non-destructive testing method for detecting objects underground and assessing, among others, pavement material layer thickness and properties [3]. It provides a capability of collecting layer thickness data at short spatial intervals and at high speed conditions.

Different researchers have reported various performances of the GPR measurements, depending on the surveyed pavement structure and the utilized data anal-

ysis methods [25]. For example, Maser reported a thickness accuracy of 7.5% for asphalt pavement layers ranging from 51 to 500-mm thick, and 12% for granular base layers ranging from 150 to 330mm thick [5].

In another research, Lahouar reported a 6.7% error for estimating the thickness of a pavement approaching its service life, which used GPR to assess the condition of a four-lane, 17-mile section of Interstate I-81 in Virginia [4]

In this thesis, GPR detection system is placed. The system could provide the accurate thickness estimation and dielectric values for a certain GPR signal. The researcher tried to extracted the surface layer thickness from GPR data. Besides, It has been placed detection methods for possible selected material for base-course layer. Finally, estimated results showed a satisfactory accuracy, which proved that the system and methods could be applied for the detection of thicknesses and defects of asphalt pavement.

1.2 STATEMENT OF THE PROBLEM

Currently, agencies in Ethiopia evaluate layer thickness and the properties of different pavement layers through the destructive process of extracting pavement cores. While this procedure provides relatively accurate thickness measurements, but it is tedious, hazardous, requires traffic control, provides limited information (as cores are usually taken every (50m-100m)).

From Ground Penetrating Radar (GPR) data, it is possible to estimating asphalt pavement thickness and material classification. However, thickness estimation, classification of the material type is not easy task due to the limitation of GPR resolution and the similar permittivity of asphalt pavement sub-layer.

1.3 OBJECTIVE

1.3.1 *General Objective*

The general objective of this study is to investigate asphalt pavement layer thickness and characteristic estimation algorithm.

1.3.2 *Specific Objectives*

The specific objectives of this thesis are:

- Explore the state of the art on thickness and characteristic estimation
- Acquire GPR data
- Analyze the data using estimation techniques.
- To estimate the dielectric constant of each layer
- To investigate the thickness of asphalt pavement
- To identify of the different layers composing a pavement

1.4 SCOPE AND LIMITATIONS

The scope of this thesis is limited to analysis of one dimensional signal space (A scan) and Two dimensional signal space (B scan). And also this thesis is limited on estimation dielectric values and thickness.

1.5 LITERATURE REVIEW

According to **Conyers , Goodman and Piro** [5], The use of ground-penetrating radar (GPR) for archaeological mapping and interpretation has evolved from a purely exploratory technique using an interpretation of two-dimensional reflection profiles to one that now commonly uses three-dimensional mapping and computer

generated visualization programs to study much larger areas of the subsurface.

According to **Lahouar, Samer** [4], start explaining why we need preprocessing: the purpose of GPR data processing is to improve the raw data quantity by manipulating the acquired data into an image that can be used to infer the subsurface structure and enhancing signal at the expense of noise; and processed signal provide velocity information, collapsing diffractions and placing digging events in their true subsurface location, increasing resolution.
He proposed to use principal component analysis (1D and 2D) and independent component analysis with ReflexW software.

To to estimate layers thickness as well as dielectric constant of each layer both time delay of backscattered echoes and dielectric constant needed. However, (**Cedric Le Bastard, Vincent Baltazart and Yide Wang**) they proposed machine learning algorithm that perfume time delay estimation of backscattered radar signals.

According to **Al-Qadi, IL and Lahouar, S** [3], raw GPR data should be first preprocessed in order to enhance its quality. The preprocessing procedure is implemented for the following benefit: to reduce noise, eliminating the undesired presence of the ground surface echo and compensating propagation losses.
He also mentions the main source of noise that might affect GPR reflected signals when performing GPR surveys along highways. Finally based on their impulse response, he proposed digital filter (Finite Impulse Response (FIR) and Infinite Impulse Response (IIR) filter) that filter out unwanted signal.

According to **Bostanudin, Nurul** [6], try to classify the target based complex natural resonance using calculated and measured examples for target identification. He proposed complex natural resonance extraction using improved Prony's method to reduce white noise.

According to **Chen, Chi-Chih and Peters, L and Burnside, Walter D** [7], the estimation of thin layer thickness performed with five different algorithm and tried to improve the time series resolution of GPR signal and presents a parametric technique.
The performance of these algorithms (i.e., Estimation of signal parameter via rotation invariance techniques (ESPRIT), Multiple signal classification (MUSIC), Min-Norm and their polynomial versions Root-MUSIC and Root-Min-Norm) were compared in terms of resolution power as well as root-mean square error on the estimated thickness.

According to **Le Bastard, Cédric** and **Baltazart, Vincent** and **Dérobert, Xavier** and **Wang, Yide** [8], try to utilizing the full waveform solution, with Backcalculation algorithm to stresses applied to the base course layer since it is deeper in the pavement.

In the GPR method, individual traces are used to produce reflection profiles, which are then resampled to generate amplitude slice maps. Each of those processing steps produces important images that must be understood, integrated, and then individually analyzed in conjunction during interpretation.
When the nature of the ground is understood and geological and archaeological reflection features are then defined and understood in three dimensions, data can

be resampled and processed to produce a meaningful final product, in this case, the amplitude slice maps and surface rendering images [9].

The related GPR thickness errors found for all test locations. These errors range between 4.62% and 8.25% for the 1 GHz antenna data, while for the 2 GHz antenna they range between 10.19% and 12.96%. For the first case,the errors are rather low and consistent with international experience, which suggests differences between thicknesses measured on core and GPR estimated thicknesses [10].

1.6 METHODOLOGY

Automating GPR data interpretation could be simplified by dividing the data analysis system into smaller subsystems. These subsystems are only interconnected by their inputs and outputs. This configuration allows the performance of each subsystem to be evaluated as if it were a standalone module.

The first step is model simulation environment by using GPRMax simulation software to acquire GPR data.Then the accrued data has to be preprocessed to cancel out the noise effect using matched filter algorithm. Finally, taking the amplitude of the incoming signal from the pavement layer(s) and the time delay; then analyze the data to estimate dielectric properties and layer thickness for each layer.

1.7 THESIS ORGANIZATION

In this study, the research work carried out is divided into different topics and presented in six chapters, they are as follows.

Chapter 1 A brief introduction, statement of the problem, and the scope is presented in the first chapter with special emphasis on the objectives of proposed study and methodology,

Chapter 2 Literature on Ground Penetrating Radar is reviewed. The chapter looks at the important parameter conducting GPRMax in and also modeling on GPRMax Simulation data using dedicated GPRMax Simulation package.

Chapter 3 Describes the methodology that tackle the problem occurred and also estimate layer thickness as well as dielectric constant.

Chapter 4 Presents Signal processing techniques used for the Asphalt pavement thickness estimation and characterization of GPRMax signals.

Chapter 5 Conclusion of the conducted research work and result are given and recommendation for future work are presented.

2

CURRENT STATE OF KNOWLEDGE

This chapter is present the working principle of Ground Penetrating Radar and its electromagnetic properties. The issues of GPR measurements and finally, its advantages disadvantage have been stated.

2.1 ELECTROMAGNETIC THEORY

The EM phenomenon can be described by four Maxwell's equations which relate the electric and magnetic fields to their sources.These were established by James Clerk Maxwell [11] based on experimental discoveries of Andre-Marie Ampere [12],Michael Faraday [13], and Carl Frierich Gauss [14]

The Maxwell's equations in integral forms in terms of total charges and currents are:

$$\oint_c \vec{H}.d\vec{l} = \frac{d}{dt}\iint_s \vec{D}.d\vec{S} + \iint_s \vec{J}_{free}.d\vec{S} \tag{2.1}$$

$$\iint_s D.d\vec{S} = \iiint_v \rho_{e,free}\, dV \tag{2.2}$$

where $\vec{D} = \epsilon\vec{E}$ is the electric flux density in $coulombs/meter^2$, ϵ is is called the permittivity of the material, $\vec{H} = \frac{\vec{B}}{\mu}$ is the magnetic field intensity in amperes/meter, and μ is called the permeability of the material. There will be conductive current given by $\vec{J} = \sigma\vec{E}$, where σ is the conductivity of a medium in siemens/meter.

Maxwell's Equations in the integral form are valid everywhere. However, the integral form is not convenient for analyzing physical problems. Therefore, it is necessary to convert them to the differential forms:

$$\nabla.\vec{E} = 0 \tag{2.3}$$

$$\nabla.\vec{H} = 0 \tag{2.4}$$

$$\nabla \times \vec{E} = \epsilon\frac{\partial\vec{H}}{\partial t} \tag{2.5}$$

$$\nabla \times \vec{H} = \epsilon\frac{\partial\vec{E}}{\partial t} \tag{2.6}$$

In the application of GPR, the object is usually in the far field region of the antenna. In the far field of an antenna, the EM field exhibits local plane wave behavior. If we assume the EM wave is propagating in the z direction, the EM filed is linearly polarized (the most general case being elliptically polarized) with an electric field only in the x direction.

2.2 GROUND PENETRATING RADAR

Ground penetrating radar technology, which has been used in civil engineering, geology and archeology since 1970s [15]. Unlike traditional radar systems, GPR systems are mainly used to detect and measure the depth of inhomogeneities in a dielectric medium. Detection could be achieved by comparing the power of the scattered EM waves produced by the contrast in the dielectric properties between medium and inhomogeneity to a prefixed threshold above the receiver noise level. Depth estimation, however, is more complicated because it requires precise measurement of the time delay between the transmitted signal and the reflected signal. The time delay can then be converted to depth by multiplying it by the speed of EM waves through the studied medium [16]

Ground penetrating radar systems are based on sending an electromagnetic wave through the surface of the ground and then analyzing the received signals collected by receiver. The propagation of electromagnetic wave through a medium depends largely on the medium's dielectric properties and structure. Therefore, to better study the propagation of GPR signals through asphalt pavements, it is necessary to start by examining the common types of asphalt pavement structure with its material property in use today.

2.3 GPR PRINCIPLES IN PAVEMENT EVALUATION

GPR systems can be divided into air-coupled and ground-coupled systems depending on the type of antennas are deployed [17].

In an air-coupled system, horn antennas are usually mounted 40 ~ 60 cm above the surface. This kind of system yields relative clean radar signals and allows for high speed road measurement (up to 100 km/h) [3].

However, the penetrating depth is usually limited to 0.5 ~ 1.0m since part of the transmitted energy from the transmitting antenna is directly reflected back into the receiving antenna by the pavement surface. In contrast, the antennas of a ground-coupled system maintain contact with the pavement surface, which yields a higher penetrating depth compared with the air-coupled systems, but the survey speed is limited [18]

For pavement surveys, air-coupled system is preferred since pavement surveys only need a relative shallow depth of penetration, and high speed surveys are more economical and convenient to survey a large area of highway. The most critical advantage of air-coupled system is allowing for estimating the dielectric constant of the different pavement layers, since the coupling pulse is separated

from the pavement surface reflection in the collected signal [19]

The typical highway pavement structure is usually divided into three layers: Hot-Mix Asphalt (HMA) layer, base layer, and subgrade layer, as depicted in Figure 2.1. The dielectric constant of HMA layer is approximately 4 ~ 8, while the dielectric values of base layer and subgrade layer are varies depend up on material composition. It means that the electromagnetic waves will reflect at the interface of two layers, which provides the physical foundation for the pavement layers detection.

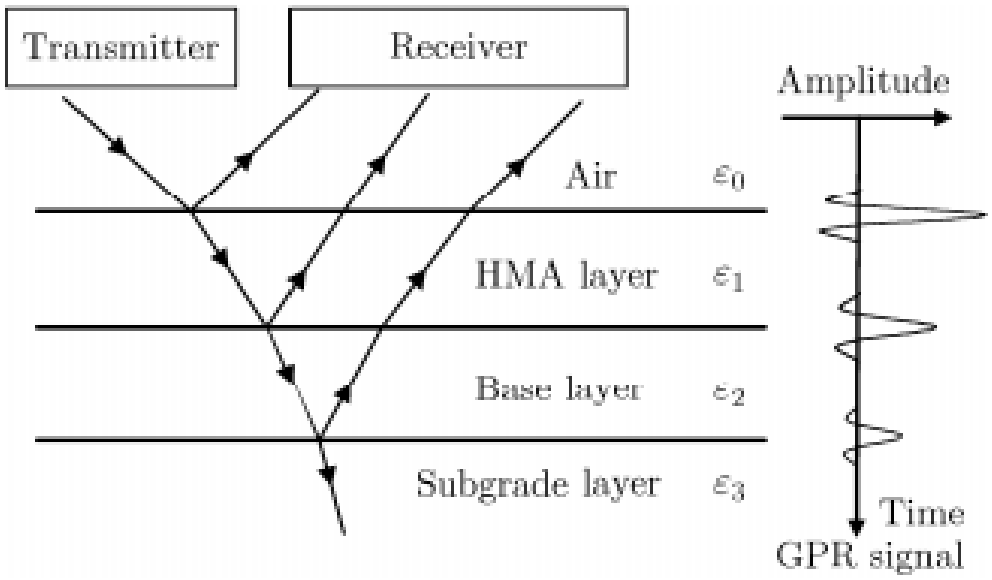

Figure 2.1: Typical pavement structure
[19]

It should be noted that in Figure 2.1, it is assumed that no multiple reflections are present within the received GPR signal, since the pavement layer interfaces are not strong reflectors [18]. In addition, the sampling time window of the GPR system is usually shorter than the time delay of multiple reflections in practical surveys, so it can be assumed that the received GPR signal is mainly composed of single reflections.

The acquired GPR signal is usually distorted due to the filter effect of the ground [20]. However, in pavement measurement applications, the shape of the received GPR signal is not significantly different from the transmitted one, since the propagation path of the electromagnetic wave is relatively short. Consequently, the received GPR signal $y_r(t)$ can be modeled as [20]

$$y_r(t) = \sum_{i=0}^{N-1} A_i(t - t_i) + n(t) \tag{2.7}$$

where x (t) represents the known transmitted GPR signal, N is the number of pavement layers, Ai denotes the amplitude of the reflected pulse at the i-th interface, n(t) is receiver noise which can be modeled as additive white Gaussian noise, and τ_i is the round-trip time delay of i-th layer.

2.4 GROUND PENETRATING RADAR ANTENNAS

Like other systems working with EM waves, a GPR system needs an antenna to transmit and receive EM energy. Depending on the number of antennas used, a GPR system can be monostatic (a single antenna is used for transmit/receive), bistatic (one antenna is used for transmission and another antenna is used for reception), or multistatic (a single antenna or multiple antennas are used as transmitters and multiple antennas are used as receivers).

In the case of a monostatic GPR, the transceiver should include a duplexer to protect the receiver from the high power signals during transmission and to direct the low power received signals to the receiver during reception.

Depending on the way antennas are deployed, GPR systems are classified as air-coupled(or launched), or ground-coupled systems. In air-coupled systems, the antennas (usually horn antennas) are typically 150 to 500mm above the surface. These systems produce a clean radar signal and allow for highway speed surveys. However, the drawback of these systems is the low depth of penetration into the pavement structure since part of the EM energy, sent by the antenna, is reflected back by the pavement surface. In contrast, a ground-coupled system's antenna is in full contact with the ground, which gives a higher depth of penetration (at the same frequency) but limits the speed of the survey. Ground-coupled antennas are usually in the form of bowtie dipoles.

For easier data interpretation, the GPR antennas are designed to radiate a wave that can be approximated in the far field ($r > 2D^2/\lambda$) by a normal-incidence transverse electromagnetic (TEM) plane wave. This applies also to the case of a bistatic configuration, where the incidence angle is small but different from zero. Moreover, the incident wave is generally linearly polarized. The half power (3dB) beamwidth varies typically between 20°and 90°.

2.5 PAVEMENT

Pavements are planar layered media with different materials composing each layer. Based on their main components, pavements are divided into three categories: [1]

- Flexible (hot-mix asphalt) pavements
- Rigid (concrete) pavements
- Composite pavements.

2.5.1 *Flexible (Hot-Mix Asphalt) pavements*

Flexible pavements are layered systems composed of different layers for different traffic loading categories. This approach allows cheaper local materials to be used in pavement construction. Table. 2.1 shows the layers which may be present in a road pavement and which may be bound with bitumen. Where thick Hot Mix Asphalt (HMA) surfacing layers are required, they are normally constructed with a

'wearing course' laid on a 'binder' course [21].

Wearing Course
Binder Course
Base Course
Sub-base

Table 2.1: Pavement Layers which Bitumen Bound

HMA surface course are the most critical layer in a pavement structure and must be of high quality and have predictable performance. It is the top layer of flexible pavement. It constructed by a dense graded hot-mix asphalt (HMA) material. This mix provides a balance in aggregate size, where a high resistance to traffic load requires large aggregate and a smooth and high resistance to deformation, low permeability to prevent the ingress of water. The surface thickness is usually varying between 50 mm - 125 mm.

Composition of HMA (Components of Mix)

The types of HMA most frequently used in tropical countries are manufactured in an asphalt plant by hot-mixing appropriate proportions of the following materials; [1]

- Coarse aggregate, defined as material having particles larger than 2.36mm;
- Fine aggregate, defined as material having particles less than 2.36mm and larger than 0.075mm;
- Filler, defined as material having particle sizes less than 0.075mm, which may originate from fines in the aggregate or be added in the form of cement, lime or ground rock; and
- A paving grade bitumen with viscosity characteristics appropriate for the type of HMA, the climate and loading conditions where it will be used.

2.5.2 *Asphalt Base course or Binder Course*

HMA layer that is composed of larger aggregates and less asphalt binder content than the surface course. Because of its low asphalt binder content, the base course resistance to fatigue cracking is less than the surface mix. The lower resistance to cracking is justified by the lower.

Base course is a layer composed of crushed stone that can be usually have thickness 170mm - 200mm.

Subbase Course is composed of selected soil for the pavement and its thickness varying between 250mm – 275mm.

As shown in the table below, different asphalt pavement materials have different dielectric constants. It should be noted, that the dielectric property of any given

Asphalt Base Course (90mm)
Base Course (170mm)
Subbase Course(175mm)
Capping Course(150mm)

Table 2.2: (a)

Asphalt Base Course (125mm)
Base Course (200mm)
Subbase Course(275mm)

Table 2.3: (b)

Table 2.4: Pavement types (a) Four Layer Asphalt (b) Three Layer Asphalt

materials is crucial to radar evaluations. Without the change in dielectric constant between materials, radar technology would not be able to determine the interface between different layers.

Material	Dielectric Values
Air	1
Water	81
Asphalt wet	9
Asphalt dry	3
Gold	44.2
Sand dry	4.5
Concrete dry	7
Sea water	8
Granite wet	7
Ice	4
Limestone dry	7
Sand Dry	3-5
Granite dry	5

Table 2.5: Dielectric Constants [22]

2.6 RIGID PAVEMENTS

Rigid pavements are constructed of 150mm to 300mm thick (6in to 12in) Portland cement concrete (PCC) slabs as illustrated in Figure 2-1c. The slabs can be placed either directly on the prepared subgrade surface or on a 100mm to 300mm thick (4in to 12in) granular base layer. Four types of PCC pavements can be identified based on the reinforcement configuration [Huang, Y. H., Pavement Analysis and Design, Prentice Hall, New Jersey, 1993]

- Jointed Plain Concrete Pavements (JPCP), shown in Figure 2-2a, are non-reinforced concrete slabs separated by transversal contraction joints to allow for concrete expansion caused by environmental conditions. The joint spacing used in these pavements is typically between 5m and 10m (15ft to 30ft).
- Jointed Reinforced Concrete Pavements (JRCP), shown in Figure 2-2b, are concrete slabs reinforced by a wire mesh or deformed bars. The reinforcement introduced in this case does not improve the structural capacity of the pavement, but rather protects the concrete against concrete shrinkage and temperature variation cracking. Thus, it increases the joint spacing, which can vary in this case from 10m to 30m (30ft to 100ft).
- Continuous Reinforced Concrete Pavements (CRCP), shown in Figure 2-2c, are reinforced by steel reinforcing bars (rebars) in the longitudinal and transversal directions. Use of reinforcement in this case eliminates the contraction joints, which are the main weakness in concrete pavements; moreover, it reduces the thickness of the slab.
- Prestressed Concrete Pavements (PCP), shown in Figure 2-2d, are built in such a way that a compressive stress is naturally imposed on the slabs in the absence of any traffic load. Consequently, tensile stresses applied by vehicles on the concrete slab will be greatly reduced, which in turn reduces pavement damage. This is based on the fact that concrete is strong in compression but weak in tension. Concrete is typically prestressed using post-tensioned steel wire strands.

Rigid pavement distresses are essentially due to repeated traffic loading and to varying environmental conditions. These distresses may be divided into two categories: distresses caused by the base (or subgrade) layer failure and distresses originating in the concrete slab itself.
The first category is caused by weakening of the base (or subgrade) layer either due to moisture accumulation or material loss produced by soil and particle pumping at the slab joints or the existing cracks. The second category can be due to the corrosion of the steel rebar in reinforced concrete, joint faulting, freezing and thawing, alkali-silica reaction in concrete, and/or other chemical attacks.

2.7 COMPOSITE PAVEMENTS

Composite pavements are composed of concrete slabs overlaid by HMA, thus providing the simultaneous strength of concrete as a base layer and the smoothness

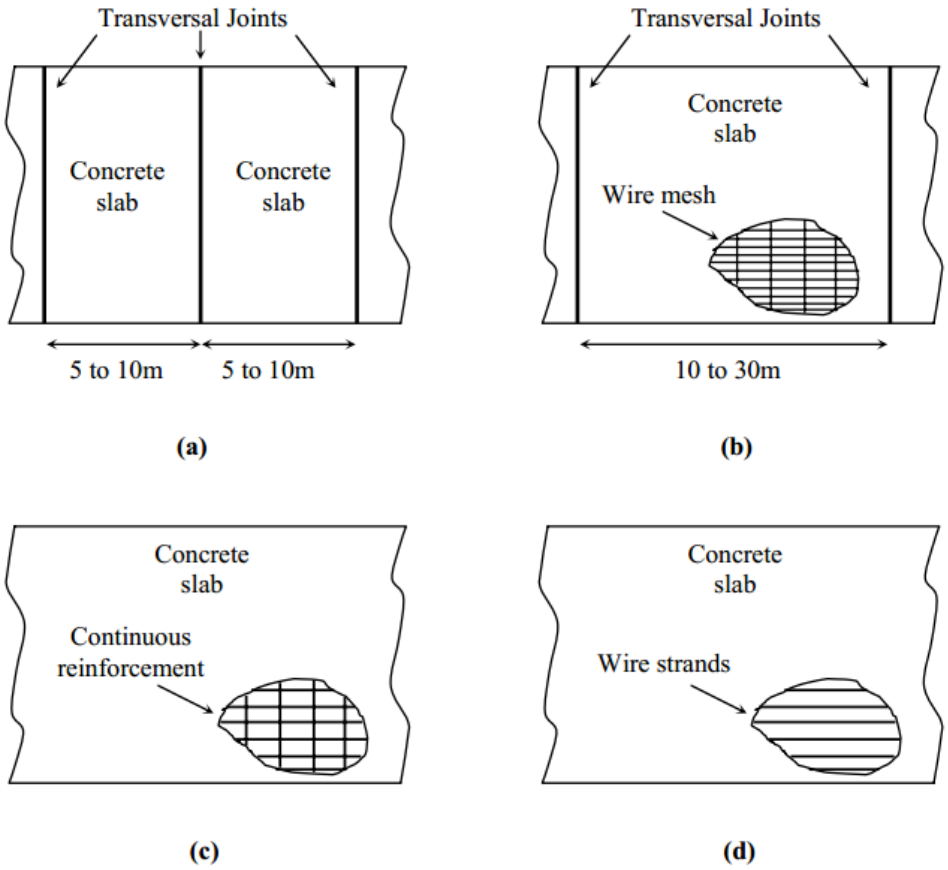

Figure 2.2: Four Different Types of Concrete Pavements: (a) JPCP, (b) JRCP, (c) CRCP, (d) PCP

[6]

of HMA. Due to the high cost of such pavements, they are rarely constructed as new pavements; however, they usually result from the rehabilitation of old concrete pavements by adding an HMA overlay at an appropriate thickness. Flexible pavements may also be overlaid with concrete, which is known as whitetopping.

Distresses in composite pavements are similar to those found in flexible pavements. However, a characteristic crack type, the joint reflection cracking, is usually found in HMA layers overlaying jointed concrete slabs. This type of cracking starts at the concrete joints and propagates over time towards the surface.

2.8 GPR DATA PRESENTATION TYPES

GPR data can be represented in three different forms: A-scan, B-scan and C-scan

A-Scan

A-Scan is a one-dimensional plot and also called a trace. It is a sequence of sample points collected by the GPR at a fixed antenna position that indicates a time variation of the recorded signal amplitude [9]. It uses to show a plot the time history for the electric and magnetic field components, and currents for all receivers in a

model (each receiver gets a separate figure window) [23].

B-Scan

B-Scan is a two-dimensional plot representing an ensemble of A-scans as GPR moves in a straight line above the ground surface. The horizontal axis represents the scan length or number of traces, whereas the vertical axis represents the range or the time elapsed for the pulse to return.

C-Scan

C-Scan is a three-dimensional display of GPR data resulting from the side-by-side arrangement of stacked B-scans. It is also represented by a collection of horizontal slices where each slice corresponds to a particular depth or a certain sample point.

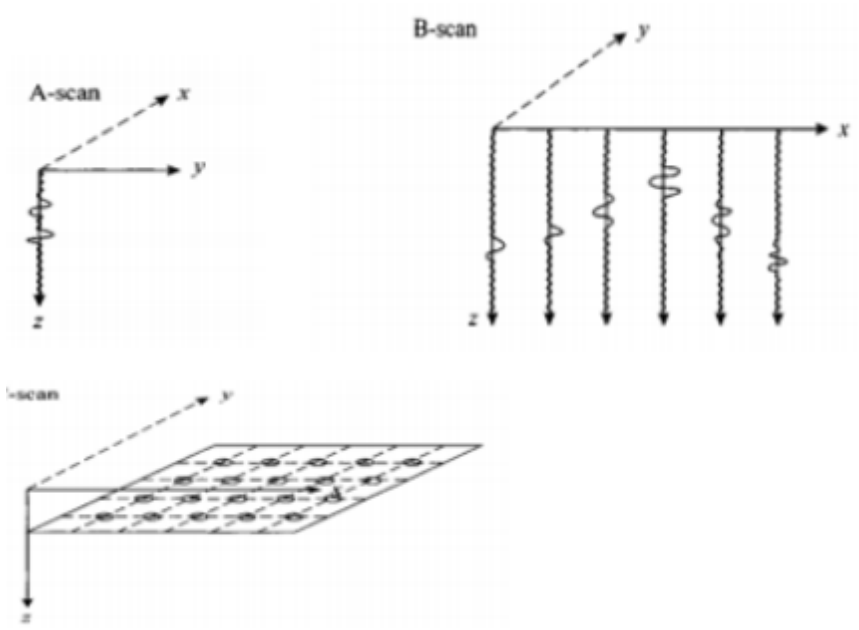

Figure 2.3: Co-ordinate systems for scan description
[3]

2.9 MATERIAL PROPERTIES

The subject of electrical properties (ϵ, μ , σ) of materials is wide- ranging topic.Background can be found in [24].Discussion here is limited to the common basic issues. In most GPR applications,variations in , and σ are most important while variations in μ are seldom of concern.

Ground penetrating radar is most useful in low-electrical-loss materials. If $\sigma = 0$,GPR would see very broad use since signals would penetrate to great depth. In practice, low-electrical-loss conditions are not prevalent. Clay-rich environments or areas of saline groundwater can create conditions where GPR signal penetration is very limited [25]. Earth materials are invariably composites of many other

materials or components. Water and ice represent the few cases where a single component is primarily present. A simple beach sand is a mixture of soil grains, air, water, and ions dissolved in water. Soil grains will typically occupy 60-80% of the available volume. Under- standing the physical properties of mixtures is thus a key factor in the interpretation of a GPR response [25].

2.9.1 *Electromagnetic Properties in Dielectric Material*

The interactions of EM waves with physical media can be quite complex and the most exact models known for EM interactions use quantum mechanics [26]. The approximation to the quantum representation is given by Maxwell's equations describing the EM interactions in terms of electric (Electric (E)) and magnetic (Magnetic (H)) field vectors that propagate and reflect as waves [24]. Often, the propagation of EM waves can be represented by scalars instead of vectors, which simplifies the mathematics at the expense of a loss in directional information, such as polarization.

Magnetic Permeability (μ)

Magnetic permeability (μ) describes the ability of a material to become magnetised in the presence of an EM field. It is a measure of the magnetic polarisation of a material that measured in henries per metre (H/m) . Materials that are more magnetically permeable will more readily interfere with the magnetic part of the EM wave, thereby attenuating the wave and resulting in shallow subsurface images. The relative permeability, μ_r of a material is given as,

$$\mu_r = \frac{\mu}{\mu_o} \tag{2.8}$$

where μ_o represents the permeability of free space and is given as,

$$\mu_o = 4\pi * 10^{-7} = 1.256 * 10^{-6} H/m \tag{2.9}$$

in which left the relative permeability with a unit-less quantity.

The relative permeability of a material is the ratio of its permeability to that of free space, and is a unitless quantity. Magnetic permeability has little effect on the propagation of a GPR wave and therefore, the magnetic permeability of subsurface materials is often assume velocity and attenuation. They are also considered to be magnetically lossy and may have a frequency dependent permeability. For ferromagnetic materials, the permeability can have an imaginary component. Soil and subsurface materials are mainly non ferromagnetic ($\mu_r \simeq 1$)), therefore, they are assumed to be the same as free space ($\mu_r = 1$) [27].

Electrical Conductivity (σ)

Electrical conductivity (σ) describes the ability of a material to conduct the electric

portion of the EM wave and is measured in Siemens per metre (S/m) . Materials which are more electrically conductive will more readily conduct the electric part of the EM wave, thereby dissipating or attenuating the wave and resulting in shallow subsurface images. Conversely, materials with a low electrical conductivity will allow greater depth of EM wave permeation [5], [24].

Since GPR is an EM energy, it is subject to attenuation (natural absorption) as it moves through a material [28]. The signal is able to penetrate a great deal of material if the energy is moving through a resistive (low conductivity) material such as very dry sand, ice, or dry concrete which makes the signal stays intact longer, thus being able to go further into the material. However, if the material is conductive such as salt water and wet concrete, the GPR energy will get absorbed before it has had the chance to go very far into the material. As a rule of thumb based on this electrical conductivity, the greater the water content of the material, the greater the conductivity.

Electromagnetic scattering

Electromagnetic scattering occurs when an incident wave encounters a discontinuity in the electromagnetic properties of the traversed medium. In the case of GPR surveys on pavements, the discontinuity can be either the interface between two layers in the pavement system or an irregularly shaped defect within a layer. Due to the discontinuity, the wave is reflected, refracted, or diffracted depending on the geometry of the diGuidance on GPR modellings continuity, the properties of the materials, and the wavelength of the incident signal. Wave scattering is generally tightly related to the problem geometry; thus, the solutions are problem specific. Since pavements are planarly layered media, only scattering from planar interfaces will be presented.

Permittivity (ε)

The permittivity (ε) [24], [28] describes the ability of a material to store and transmit an electric charge induced by an EM field that measured in Farads per meter (F/m) . It is a descriptive number that indicates how fast radar energy travels through a material. Radar energy will always move as quickly as possible through a material, but certain materials slow down the energy more than others. The speed moving GPR energy can be deduced by knowing the value of permittivity, e.g. the higher the permittivity, the slower the radar wave moves through the medium. The wet material will for example slow down the radar signals due to the water presence causing the raise of the overall dielectric of the materiaGuidance on GPR modellingl.

The permittivity of free space ε_o is assumed to be the same as in a vacuum which is,

$$\varepsilon_o = \frac{1}{c^2 \mu_o} = 8.854 * 10^{-12} \mathrm{F/m} \tag{2.10}$$

The relative permittivity ε_r of a material is therefore can be considered as in equation (2.4) and is unit-less.

$$\varepsilon_r = \frac{\varepsilon}{\varepsilon_o} \tag{2.11}$$

2.10 DATA COLLECTION PARAMETERS

here are numerous other parameters that can be varied and controlled to achieve the targeted depth and resolution during a GPR survey. These parameters are described in the following section.

2.10.1 *Wave velocity*

The angular frequency (ω) [29] of an EM wave is measured in radians per second (rads/s) and is proportional to its frequency, f measured in Hertz:

$$\omega = 2\pi f \tag{2.12}$$

The wave number, or propagation constant,(β) is measured in radians per meter and is given by [30]:

$$\beta = \omega\sqrt{\frac{\mu\varepsilon}{2}[\sqrt{1+[\frac{\sigma}{\omega\varepsilon}]^2}+1]} \tag{2.13}$$

For the material with no conductivity, equation (2.6) can be reduced to:

$$\beta = \omega\sqrt{\mu\varepsilon} \tag{2.14}$$

The velocity at which a wave travels through a material (v)is measured in meters per second and is given by [30]:

$$v = \frac{\omega}{\beta} \tag{2.15}$$

The wave velocity of free space (c) can be obtained from the equations (2.7) and (2.8) respectively [29]:

$$c = \frac{\omega}{\beta_o} = \frac{\omega}{\mu_o \varepsilon_o} = 3 * 10^8 m/s \tag{2.16}$$

For materials with no conductivity ($\varepsilon = 0$) and permeability equals to that of free space ($\mu_r = 1$) , equation (2.9) can be stated as:

$$v_r = \frac{\omega}{\beta} = \frac{1}{\sqrt{\mu_r \mu_o \varepsilon_r \varepsilon_o}} = \frac{c}{\sqrt{\varepsilon_r}} \tag{2.17}$$

2.10.2 *Wavelength*

Wavelength λ [29] can be described as a propagating wave which repeats itself at a particular distance and is measured in meters:

$$\lambda = \frac{2\pi}{\beta} = 2\pi\frac{v}{\omega} = \frac{v}{f} \tag{2.18}$$

GPR antennas can typically be distinguished when moving along the concrete features aligned perpendicular to the direction of travel if they are spaced at least one half of a wavelength apart ($\lambda/2$) . Features that are stacked on top of each other can typically be distinguished if they are at least a quarter of a wavelength apart ($\lambda/4$) [28] . However, features that are closer to each other than these distances may appear as a single feature in GPR data.

2.10.3 *Relationship Between Frequency and Depth*

Choosing a frequency for a GPR survey is quite critical. Lower frequency with long wavelengths provide the deepest penetration, whereas high frequency with short wavelengths are only able to image shallow features [5], [31], [32]. Resolution of subsurface features is in part affected by antenna wavelength which is also directly related to the frequency. Higher frequency radar provides higher resolution than lower frequency radar [32], [33]. The shorter wavelengths of high frequency produce a narrower cone of transmission and give the ability to focus on smaller areas, thereby resolve smaller features. This is differs to lower frequency radar which has more spread out transmission cones due to longer wavelengths [5].

2.11 ADVANTAGE AND DISADVANTAGE OF GPR

The major GPR strengths, on which its success in the civil engineering field is based, has several beneficial advantages [2],[21].

- The non-destructiveness and non-intrusiveness of the surveys
- Notably lower costs compared to traditional methods
- The capability of characterizing both metallic and non-metallic targets
- High-speed data acquisition, reliability and representativeness of measurements.
- Its ability to maximize research efficiency and minimize the cost

Despite of its advantages described earlier, GPR has some limiting factors [6].

- Some soils like saline, shale or clay have high conductivity, which limits the GPR from penetrating the soil.
- High frequency GPR antennas (300-1000+ MHz) can only penetrate a short distance down
- A general rule applied when using ground penetrating radar, is that, for every foot in depth, the buried utility must be an inch in diameter. For example, a six-foot deep pipe would need to be at least 6" in diameter to locate it via GPR.
- Soil density, location accessibility and crowding of surrounding utilities can also affect the GPR's success.
- Operating this equipment and understanding the results require experience and extensive training because the equipment is non-intuitive to most beginners.
- Limited resolution
- Needs Professional to interprate data

On the other hand, infrared thermography has been applied to infrastructures not only for pavement quality control [34], but also for the analysis of use by controlling both traffic flow and pedestrians [34]; and for quality control of structures such as bridges (especially moisture detection), that present high susceptibility to moisture content [35], [36], both as a stand-alone technique and already combined with GPR.

Infrared thermography is a technique based on the fact that bodies at temperatures over 0 K emit radiation in the infrared wavelength of the spectrum, proportionally to their temperatures. Since defects present a different temperature to unaffected areas, they are easier to detect the greater this temperature difference is.

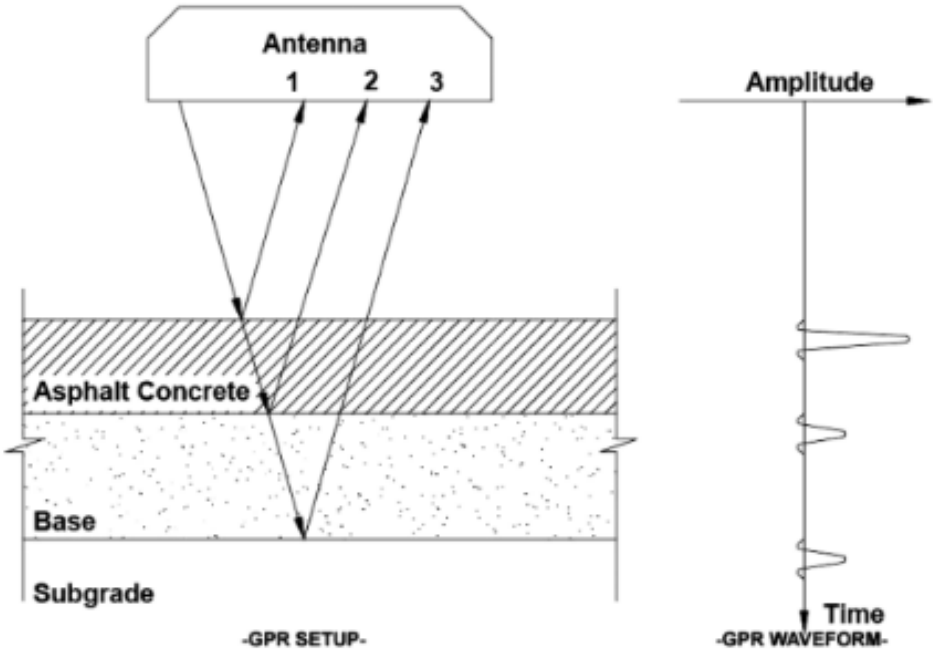

Figure 2.4: The GPR principle for pavements
[20]

Figure. 2.2 shows, an example for the case of a typical asphalt pavement, where the reflections from the top of the AC layer,the AC/base layers interface, and the base/subgrade layers interface are recorded.

Figure. 2.3 shows the geometry of the antenna and the GPR ray paths. The reflected pulses are received by the antenna and recorded as waveform. As the sensor equipment travels along the pavement, it generates a sequence of wave forms. The recorded reflections depend on the velocity of the waves propagation (see Figure. 2.3), which is governed by the electromagnetic properties of the materials [37]. It is worthwhile to mention that following the principles of the multilayer theory for pavement analysis [38], the AC pavement material is considered as isotropic.

Figure. 2.4, [39], shows that the waves propagation is taken along the axis, while the Electric Field (E) and Magnetic Field (H) are perpendicular. As considered in this figure, in free space, the magnetic susceptibility and electric permittivity are

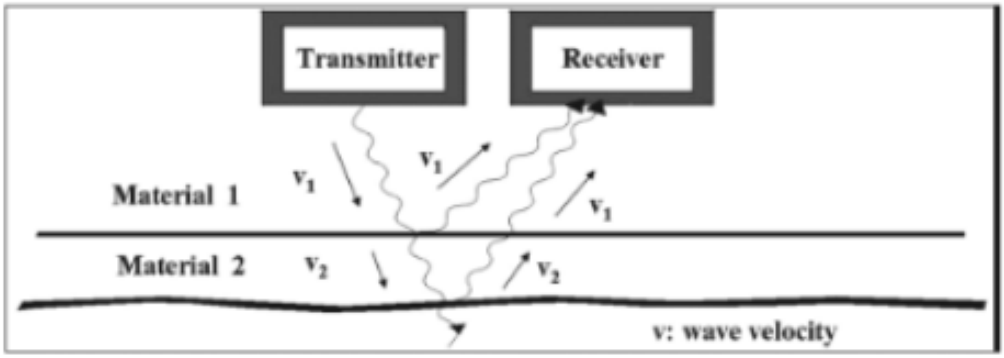

Figure 2.5: Determination of pavement layer thickness.
[20]

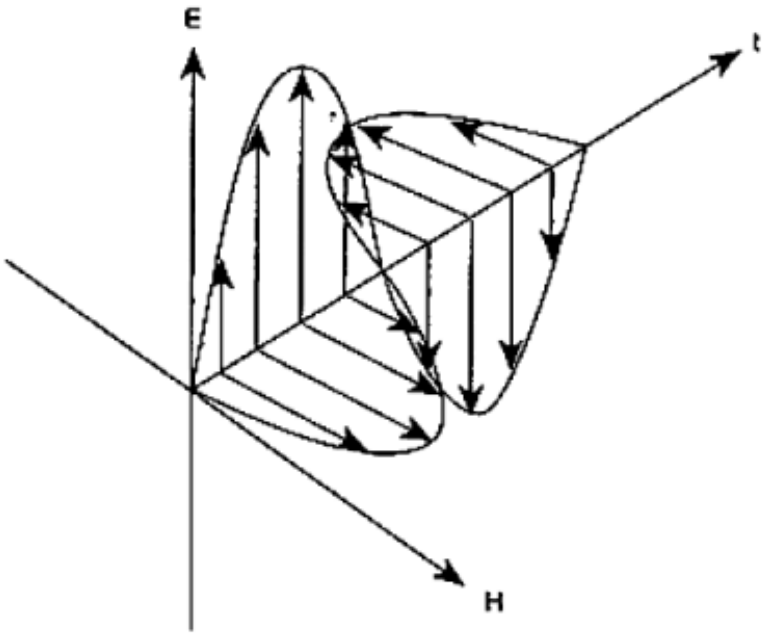

Figure 2.6: The GPR principle for pavements
[20]

independent of frequency and the medium is not dispersive. Hence, no attenuation of the waves is encountered, which happens in real dielectric medium. The wave propagation can be represented by the one-dimensional wave equation of the following form:

$$\frac{\partial^2 E}{\partial z^2} = \mu.\varepsilon \frac{\partial^2 E}{\partial t^2} \tag{2.19}$$

where μ and are " the magnetic susceptibility and dielectric values of the medium, respectively. The dielectric value is the ratio of the material electric field capacity to that of free space. It can be considered that the dielectric value of a purely dry asphalt core results from the combination of the volumetric ratio of asphalt, air

and aggregate, and their individual dielectric values.

The dielectric value of Asphalt Concrete pavement materials is often correlated with the density, air voids, asphalt content, and moisture accumulation as stated among others by [40] and [41].

2.12 GUIDANCE ON GPR MODELLING

In order to make the most of GPRMax for modelling GPR you should be familiar with the Finite-Difference Time-Domain (FDTD) method on which the software is based.
This section discusses some basic concepts of the FDTD method and GPR modelling. There is a large amount of further information available in the relevant literature.Good starting points are [42] and [43], and the specific application of FDTD to the GPR forward problem is described in [44].

2.12.1 *Basic Concepts*

All electromagnetic phenomena, on a macroscopic scale, are described by the well-known Maxwell's equations. These are first order partial differential equations which express the relations between the fundamental electromagnetic field quantities and their dependence on their sources.

$$\nabla \times E = \frac{\partial B}{\partial t} \tag{2.20}$$

$$\nabla \times H = \frac{\partial D}{\partial t} + J_c + J_s \tag{2.21}$$

$$\nabla \cdot B = 0 \tag{2.22}$$

$$\nabla \cdot D = q_v \tag{2.23}$$

where t is time (seconds) and q_v is the volume electric charge density (coulombs/cubic meter). In Maxwell's equations, the field vectors are assumed to be single-valued, bounded, continuous functions of position and time. In order to simulate the GPR response from a particular target or set of targets the above equations have to be solved subject to the geometry of the problem and the initial conditions.

The nature of the GPR forward problem classifies it as an initial value – open boundary problem. This means that in order to obtain a solution you have to define an initial condition (i.e. excitation of the GPR transmitting antenna) and allow for the resulting fields to propagate through space reaching a zero value at infinity

since, there is no specific boundary which limits the geometry of the problem and where the electromagnetic fields can take a predetermined value. Although the first part is easy to accommodate (i.e. specification of the source), the second part cannot be easily tackled using a finite computational space.

The FDTD approach to the numerical solution of Maxwell's equations is to discretize both the space and time continua. Thus the discretization spatial $\triangle x$, $\triangle y$ and $\triangle z$ and temporal $\triangle t$ steps play a very significant role – since the smaller they are the closer the FDTD model is to a real representation of the problem. However, the values of the discretization steps always have to be finite, since computers have a limited amount of storage and finite processing speed. Hence, the FDTD model represents a discretized version of the real problem and is of limited size. The building block of this discretized FDTD grid is the Yee cell [45] named after Kane Yee who pioneered the FDTD method. This is illustrated for the 3D case in Figure 2.5 . By assigning appropriate constitutive parameters to the locations of the

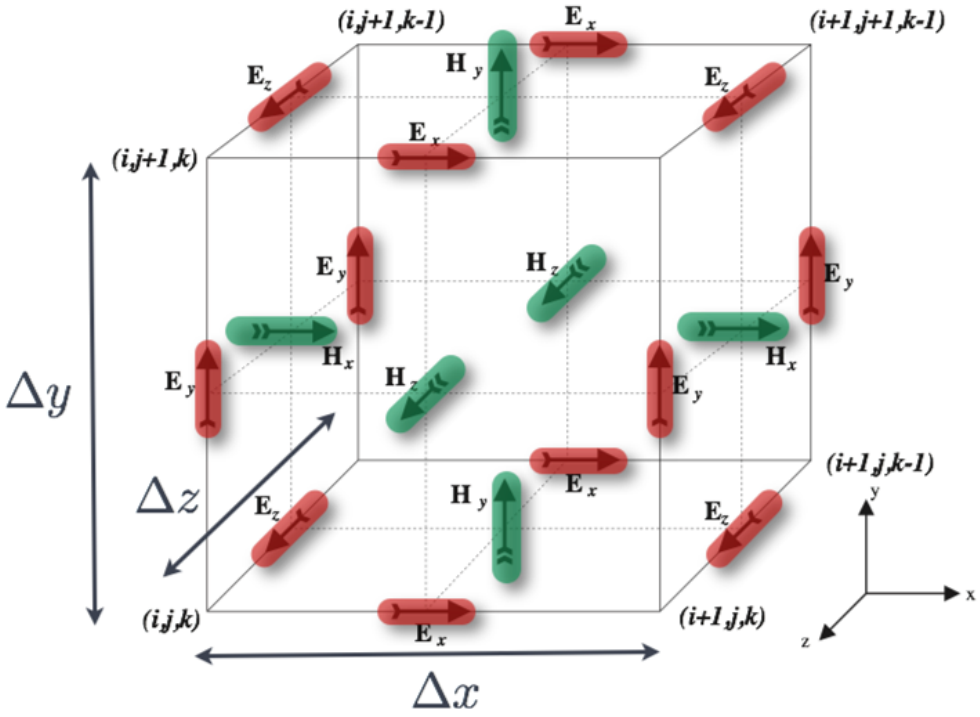

Figure 2.7: Single FDTD Yee cell showing electric (red) and magnetic (green) field components.

[45]

electromagnetic field components complex shaped targets can be included easily in the models. However, objects with curved boundaries are represented using a staircase approximation.

GPRMax is fundamentally based on solving Maxwell's equations in 3D using the FDTD method - transverse electromagnetic (TEM) mode. However, it can also be used to carry out simulations in 2D using the transverse magnetic (TM) mode. This is achieved through specifying a single cell slice of the domain, i.e. one dimension

of the domain must be equal to the spatial discretization in that direction. When this occurs the electric and magnetic field components on the two faces of single cell slice in the invariant direction are set to zero. This is illustrated for the 2D TMz case in Figure 2.6.

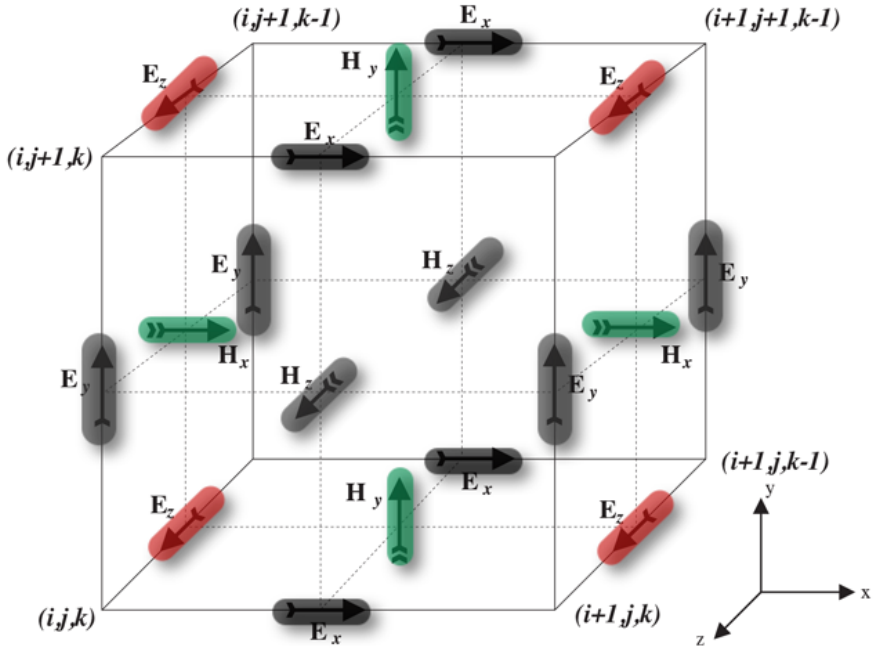

Figure 2.8: Single FDTD Yee cell showing electric (red), magnetic (green), and zeroed out (grey) field components for 2D transverse magnetic (TM) z-direction mode. [45]

Using this approach means that Maxwell's equations in 3D, shown in (1) as six coupled partial differential equations, reduce to the corresponding 2D form - in this case 2D TMz, shown in (Figure 2.6).

$$\frac{\partial E_x}{\partial t} = \frac{1}{\varepsilon}\left(\frac{\partial H_z}{\partial y} - \frac{\partial H_y}{\partial z} - J_{sx} - \sigma E_x\right) \tag{2.24}$$

$$\frac{\partial E_y}{\partial t} = \frac{1}{\varepsilon}\left(\frac{\partial H_x}{\partial z} - \frac{\partial H_z}{\partial x} - J_{sy} - \sigma E_y\right) \tag{2.25}$$

$$\frac{\partial E_z}{\partial t} = \frac{1}{\varepsilon}\left(\frac{\partial H_y}{\partial x} - \frac{\partial H_x}{\partial y} - J_{sz} - \sigma E_z\right) \tag{2.26}$$

$$\frac{\partial H_x}{\partial t} = \frac{1}{\mu}\left(\frac{\partial E_y}{\partial z} - \frac{\partial E_z}{\partial y} - M_{sx} - \sigma^* H_x\right) \tag{2.27}$$

$$\frac{\partial H_y}{\partial t} = \frac{1}{\mu}(\frac{\partial E_z}{\partial x} - \frac{\partial E_x}{\partial z} - M_{sy} - \sigma^* H_y) \tag{2.28}$$

$$\frac{\partial H_z}{\partial t} = \frac{1}{\mu}(\frac{\partial E_x}{\partial y} - \frac{\partial E_y}{\partial x} - M_{sz} - \sigma^* H_z) \tag{2.29}$$

$$\frac{\partial E_z}{\partial t} = \frac{1}{\varepsilon}(\frac{\partial H_y}{\partial x} - \frac{\partial H_x}{\partial y} - J_{sz} - \sigma E_z) \tag{2.30}$$

$$\frac{\partial H_x}{\partial t} = \frac{1}{\varepsilon}(\frac{\partial E_z}{\partial y} - M_{sx} - \sigma^* H_x) \tag{2.31}$$

$$\frac{\partial H_y}{\partial t} = \frac{1}{\varepsilon}(\frac{\partial E_z}{\partial x} - M_{sy} - \sigma^* H_y) \tag{2.32}$$

These equations are discretized in both space and time and applied in each FDTD cell. The numerical solution is obtained directly in the time domain in an iterative fashion. In each iteration the electromagnetic fields advance (propagate) in the FDTD grid and each iteration corresponds to an elapsed simulated time of one $\triangle t$.

The price you have to pay for obtaining a solution directly in the time domain using the FDTD method is that the values of $\triangle x$, $\triangle y$ and $\triangle z$ and $\triangle t$ can not be assigned independently. FDTD is a conditionally stable numerical process. The stability condition is known as the CFL condition after the initials of Courant, Freidrichs and Lewy and is given by,

$$\triangle t \leqslant \frac{1}{c\sqrt{\frac{1}{(\triangle x)^2} + \frac{1}{(\triangle y)^2} + \frac{1}{(\triangle z)^2}}} \tag{2.33}$$

where cc is the speed of light. Hence $\triangle t$ is bounded by the values of $\triangle x$, $\triangle y$ and $\triangle z$. The stability condition for the 2D case is easily obtained by letting $\triangle z \to \infty$.

2.13 GPR IMAGING TECHNIQUES

Different attempts to obtain an "image" of subsurface inhomogeneities from GPR data were tried by different authors. The problem, in this case, is to find the subsurface object distribution function, which is proportional to the dielectric property distribution in the surveyed area. In fact, when displayed in 2D or 3D, the object distribution function could be considered as a good image of the subsurface objects.

Johansson and Mast [14] presented a 3D GPR imaging technique based on focusing the time domain reflected signals using Synthetic Aperture Radar (SAR) data. This technique assumes that imaging is done in a homogeneous medium with known

parameters. To get the 3D subsurface image, GPR data is collected over a grid of points covering the surveyed area. The object distribution function is then obtained by averaging all the reflected signals at the point of interest. The averaging procedure should take into account the time delay between the antenna position where the reflected signal was collected and the point of interest in the distribution function.

Devaney [46] used diffraction tomography techniques to create images of weak reflective inhomogeneous formations in a homogeneous background using GPR. The technique is based on linearizing the wave equation's solution, which has an integral form in this case. This equation expresses the scattered field at any point in space as a function of the inhomogeneity object distribution function and the field within the inhomogeneity. The linearization uses either the Born or the Rytov approximation for weak scatterers. These approximations assume that the scattered field is small compared to the incident field, which requires the magnitude of the object distribution and the total volume of the object to be small. This second condition could be relaxed with the Rytov approximation. After linearization, the object distribution function would be linearly related to the scattered field when the Born approximation is applied, and to the complex phase of the scattered field when the Rytov approximation is applied. With these two approximations, the object distribution function is solved by a simple matrix inversion.

Johansson and Mast [47] used a GPR imaging technique based on diffraction tomography. The algorithm used in this technique tries to find the spatial distribution of a buried object from the reflected waves by using a plane-to-plane backward propagation technique that is based on a spatial linear filter. The results found for each frequency component of the reflected signal are then superimposed to give the global solution. It should be noted that, in this case, GPR data is acquired within a rectangular area (2D) rather than along a longitudinal line.

3

SYSTEM MODEL

This chapter will present about methods that has been used to estimate asphalt pavement thickness and material characterization and noise reduction method also described. Finally, introducing the flow chart for each sub-step with description. gprMax simulation software package will be introduced.

Automating GPR data interpretation could be simplified by dividing the data analysis system into smaller subsystems. These subsystems are only interconnected by their inputs and outputs. This configuration allows the performance of each subsystem to be evaluated as if it were a standalone module. Moreover, it allows for the evaluation of any combination of consecutive subsystems. Another advantage of this configuration is the possibility of distributing the data processing over multiple processors to speed up the analysis.

The flowchart of the proposed data analysis system is depicted in Figure 3.1. The system includes the following components:

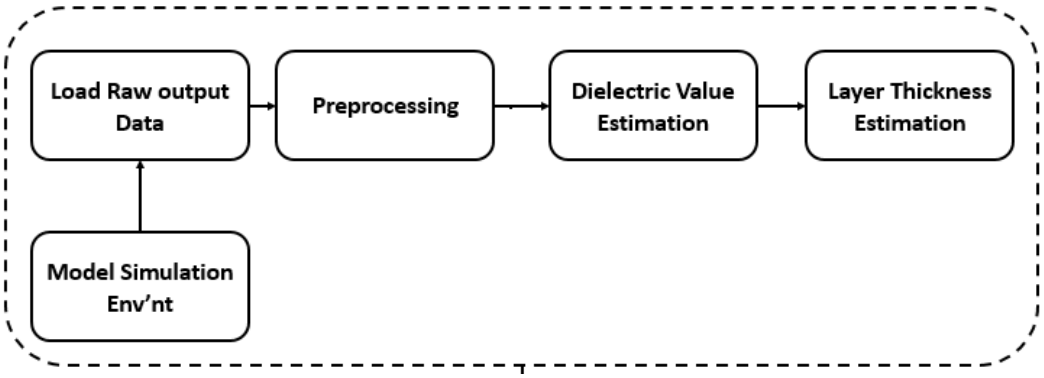

Figure 3.1: Overall Process
[16]

3.1 FDTD SIMULATION

The FDTD method is a computational EM technique that solves Maxwell's equations step by step in time domain [48]. In this research, a 2-D and 3-D FDTD simulation was conducted to simulate GPR signals reflected from asphalt pavement to estimate asphalt dielectric values and thickness.

3.2 SIGNAL PRE-PROCESSING TECHNIQUES

Raw GPR(GPRMax) data should be first preprocessed in order to enhance its quality. Preprocessing mainly because the received data consists of four signal compo-

nents, antenna cross-talk. Air-ground interface reflection, the background resulting from scatterers within each layer scattered signal. Two of them, noise and antenna cross-talk can be reduced by proper system design (i.e. using shielded antenna) or by proper signal processing [15].
Using gprMax user guide [23], started to create the model (asphalt pavement) which having three layers with different dielectric properties and used 1.5GHz air suspended GPR system.

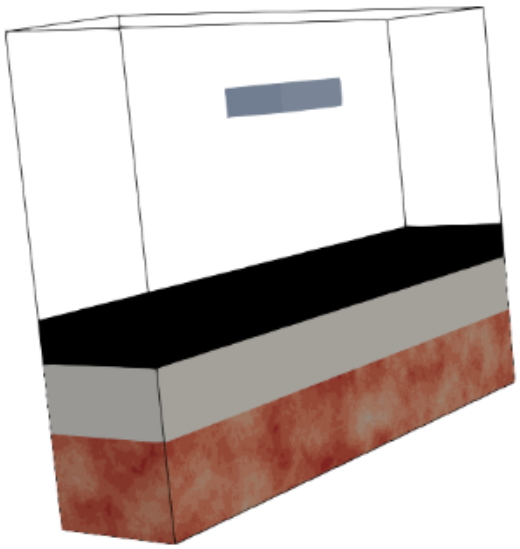

Figure 3.2: Typical Asphalt Pavement Simulated on GPRMax with Air Suspended Antenna

3.2.1 *Noise Filtering*

Because of the ultra-wide bandwidth of impulse GPR receivers, GRP signals are susceptible to noise corruption. The main source of noise that might affect GPR reflected signals when performing GPR surveys along highways are cell-phone towers, cell-phones, and any other EM devices emitting in the GPR bandwidth [26]. It should be noted that even though GPR antennas are mainly directed towards the ground, they still interfere with EM devices in their vicinity. However; for these thesis work, there is no such kinds of noise because all simulation environment was software. Furthermore, it was noticed during the simulation that different noise sources from each layer.

3.2.2 *Matched Filter Detector*

A common method for reducing the effects of random noise in signals is through the use of filters. Ground penetrating radar systems usually have digital filters implemented by a DSP processor to filter the collected data in real time. These filters are commonly set on high bandwidths to prevent the attenuation of useful data.
If $h(t)$ is the impulse response of a filter defined as the time reversal of the known

signal $x(t)$, then it could be shown that the correlation operation of equation (equation(1)) is equivalent to a filtering operation. The impulse response of the filter $h(t)$ is given by the next equation.

$$h(t) = x(T - t) \tag{3.1}$$

where T is the duration of signal x(t) introduced to make the filter h(t) causal and, therefore, realizable. Since the filter h(t) matches the signal $x(t)$, it is known as a matched filter (MF).
Hence, the optimal detector, known as a correlator detector, found based on the LRT, correlates the measured signal r with the known signal x and then compares the result to a fixed threshold St . The signal x is declared detected or not, within the signal r, depending on whether the result of the correlation is higher or lower than the threshold.

$$l(r) = r^T x > s_t \tag{3.2}$$

Applying the matched filter h (t) to the measured signal r(t) produces the output $y_{MF}(t)$, as given by next equation.

$$y_{MF}(t) = r(t) * h(t) = \sum_{\tau} r(\tau) * h(t - \tau) = \sum_{\tau} r(\tau)x(T - t + \tau) \tag{3.3}$$

It is clear from this equation that the output of the matched filter $y_{MF}(t)$ is equal to the correlation result at time T. Hence, the optimal detector of equation (Equation (3.2)) can be implemented in the form of a matched filter . Under this form, the detection decision (i.e., comparison to the threshold St is made based on the matched filter output sampled at time T.
Using these properties of the MF, the following algorithm for detecting multiple reflected pulses within the GPR reflected signal yr(t) could be derived:

1. Compute the matched filter impulse response $h(t)$ as the time reversal of the incident GPR signal $x(t)$,
2. Filter the measured GPR signal yr(t) using the matched filter $h(t)$ to obtain the filtered signal $y_{MF}(t)$,
3. Find the maximum absolute value of the matched filter output $y_{MF}(t)$
4. Compare the maximum value found to the selected threshold S_t. If the maximum value is less than the threshold, then terminate the detection procedure; otherwise, subtract the width T of the known signal $x(t)$ from the time-delay corresponding to the maximum value of the MF output to find the time-delay of the detected pulse,
5. Set the detected pulse in $yr(t)$ to zero,
6. Repeat at step 2.

3.3 GROUND PENETRATING RADAR(GPR) SYSTEM

Ground Penetrating Radar is a series of electromagnetic pulses transmitted into the asphalt pavement surface by either an air launched horn or ground coupled antenna. The transmitted pulses are reflected back to the antenna showing the asphalt pavement properties by measuring the amplitude and arrival time of the pulse. The change in the amplitude and arrival time of the pulse has a direct relationship to the change of the electrical properties of the asphalt pavement. The change of the electrical properties of the material is referred to as the change in dielectric constant[1]

GPR systems are mainly used to detect and measure the depth of inhomogeneities in a dielectric medium. Detection could be achieved by comparing the power of the scattered EM waves produced by the contrast in the dielectric properties between medium and inhomogeneity to a prefixed threshold above the received noise level. Depth estimation, however, is more complicated because it requires precise measurement of the time delay between the transmitted signal and the reflected signal.The time delay can then be converted to depth by multiplying it by the speed of EM waves through the studies medium.

3.3.1 *Layer Thickness Estimation from GPR data*

The principle of the GPR system used in this study (impulse radar) is based on sending an EM pulse through an antenna to the pavement surface and then recording the reflected pulses from the internal interfaces, where there is a contrast in the dielectric properties, as depicted in Figure 3.10. The time difference measured between the reflected pulses (i.e., t1 or t2) can be used in conjunction with the dielectric properties of the surveyed layer to determine its thickness.

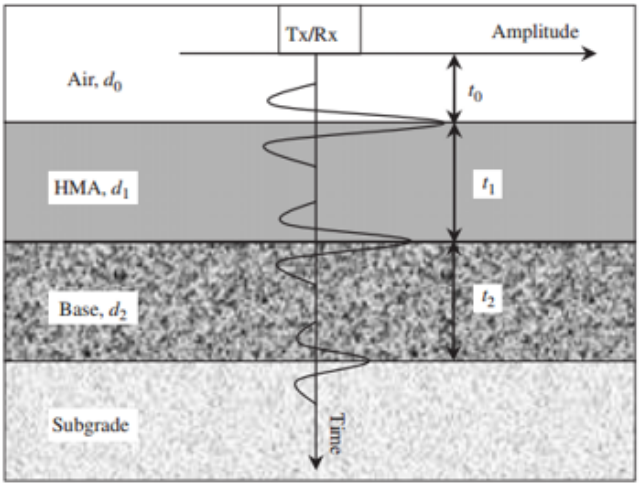

Figure 3.3: Typical GPR Reflection from asphalt pavement system [3]

The thickness of the ith layer could be computed according to the following Equation 3.10

Depending on the way antennas are used, GPR systems are classified as air-coupled or ground-coupled systems. In air-coupled systems, the antennas (usually horn antennas) are typically deployed 150–500 mm above the surface and the antennas are suspended above the pavement surface for operation at highway speeds (up to 80km/h approximately). However, because part of the EM energy sent by the antenna is reflected back by the pavement surface, the depth of penetration is limited.

In contrast, a ground-coupled systems antenna is the antennas must have a close contact to ground of a few centimeter with no need to have a direct contact which gives a higher depth of penetration (at the same frequency) but limits the speed of the survey.

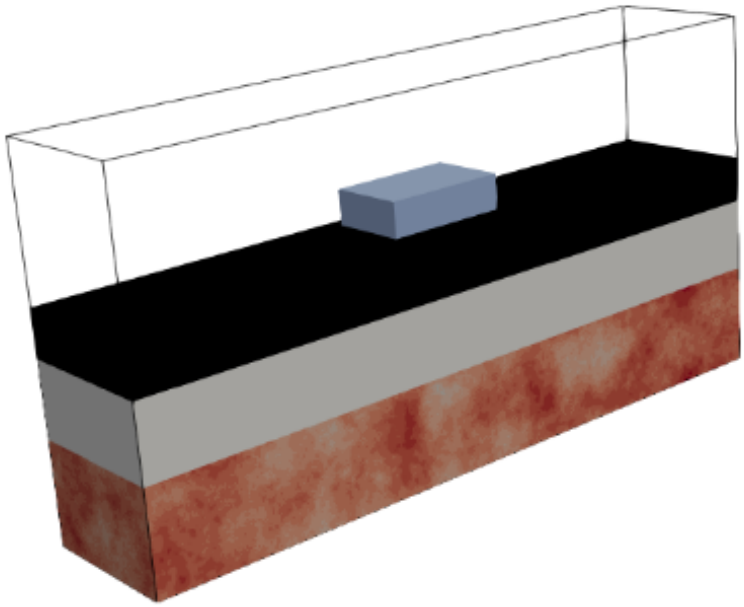

Figure 3.4: Typical Asphalt Pavement Simulated on gprMax with Ground Coupled Antenna

For practical pavement surveys, GPR antennae are typically rigidly mounted on a survey van, as depicted in Figure 3.5.

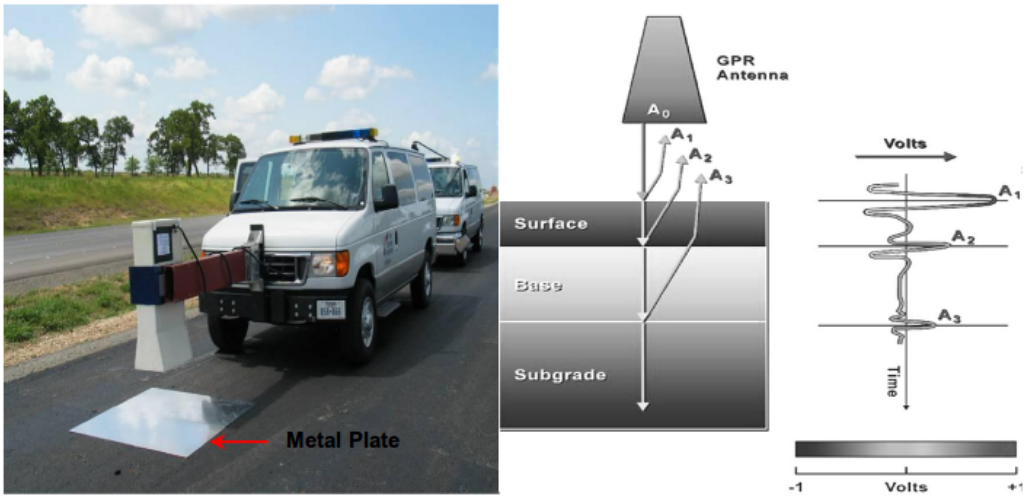

Figure 3.5: Practical GRP van used for pavement surveys showing antennae configuration [2]

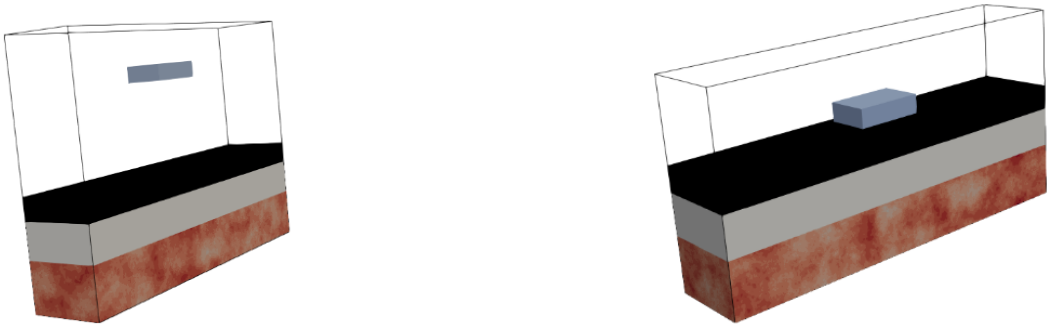

Figure 3.6: Typical Asphalt Pavement Simulated on gprMax with Air Suspended and Ground coupled antennae

This figure 3.6 shows an air-suspended system composed of a horn antennae and a ground-coupled system comprised of a single antenna.

The air-suspended systems are becoming increasingly popular for the evaluation of the upper part of the pavement structure, while the ground coupled systems are used in order to get information from the entire pavement structure up to 3m approximately [1]

3.3.2 *Layer Thickness Estimation Procedure*

The Asphalt pavement system could be modeled as set of N + 1 homogeneous planar layers, as shown in Figure 3.7. Each layer i was assumed to be a semi-infinite layer that has a finite thickness d_i, a dielectric constant ε_i, a conductivity σ, and a magnetic permeability equal to that of free space because of the nonmagnetic nature of pavement materials[49][50]. Fig.3.7 the planar layer model of asphalt pavements. γ_i, di are, respectively, the permittivity, conductivity and thicknesses as layer i, γ_i and τ_i are reflection and transmission coefficient at layer interface i.

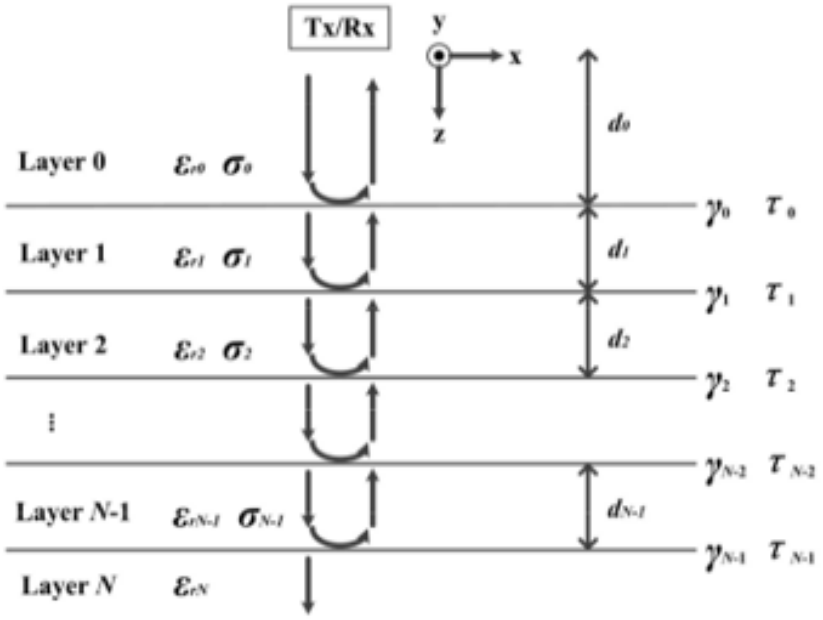

Figure 3.7: The planar layer model of asphalt pavements.(ε_i ,σ_i, di are, respectively, the permittivity, conductivity and thicknesses as layer i, γ_i and τ_i are reflection and transmission coefficient at layer interface i.
[16]

The reflection coefficients (γ_i) and transmission coefficients (τ_i) at each layer interface i could be described as follows [32]:

$$\gamma_i = \frac{\sqrt{\varepsilon_{ri}} - \sqrt{\varepsilon_{ri+1}}}{\sqrt{\varepsilon_{ri}} + \sqrt{\varepsilon_{ri+1}}} = \frac{Ai}{Am} \tag{3.4}$$

$$\gamma_i = \frac{2\sqrt{\varepsilon_{ri}}}{\sqrt{\varepsilon_{ri}} + \sqrt{\varepsilon_{ri+1}}} = 1 + \gamma_i \tag{3.5}$$

Substituting the reflection and transmission coefficients in the model yields the reflection amplitude An at interface n as Equation(3.5):

$$An = Am\frac{\sqrt{\varepsilon_{rn}} - \sqrt{\varepsilon_{rn+1}}}{\sqrt{\varepsilon_{rn}} + \sqrt{\varepsilon_{rn+1}}}[\prod_{i=0}^{n-1}(1-{\gamma_i}^2)] \tag{3.6}$$

where Am is amplitude of the incident signal.
Thus, the end result for dielectric constant of nth layer (ε_{rn}) could be found by transforming Equation (3.9), as given by the next equation:

$$\varepsilon_{rn} = \varepsilon_{rn-1}(\frac{1-(\frac{Ao}{Am})^2 - \sum_{i-1}^{n-2}(\gamma_i(\frac{Ao}{Am}) - (\frac{An-1}{Am})}{1-(\frac{Ao}{Am})^2 - \sum_{i-1}^{n-2}(\gamma_i(\frac{Ao}{Am}) - (\frac{An-1}{Am}))})^2 \tag{3.7}$$

for n =2.....N
The dielectric constant of the surface layer could be derived briefly as follows:

$$\varepsilon_{rn} = (\frac{1+\frac{Ao}{Am}}{1-\frac{Ao}{Am}})^2 \tag{3.8}$$

In order to obtain the values of the dielectric constant, we needed both the amplitudes of the surface reflected pulses and the amplitude of the GPR incident signal. However, only the amplitudes of the surface reflected pulses could be ascertained. Therefore, I designed a simulated experiment using GPRMax to get the incident signal. The GPR was placed on a large metal plate and switched to work. In this case, the amplitude of reflected signal could be considered as the amplitude of the incident signal, and then the dielectric constant could be obtained [16]. According to the calculated dielectric constant, the velocity of the electromagnetic wave propagation through the nth layer of pavement was determined as:

$$v_n = \frac{c}{\sqrt{\varepsilon}_{rn}} \tag{3.9}$$

Finally, the accurate thicknesses of asphalt pavement layers (d) could be determined from the dielectric constant (ε_r) and delay time of the latter echo relative to the former echo (t) [16]:

$$d = \frac{vt}{2} = \frac{ct}{\sqrt{\varepsilon}_{rn}} \tag{3.10}$$

3.3.3 *Percentage Relative Error*

The percent of error of a measurement is the relative error expressed as a percent.Percent of error can be used to compare different measurements because, being a percent, it compare each error in terms of 100. Relative error compares the size of the error to the size of the object being measured. When relative error given as a percent, it referred to as percent error.

Percentage Relative Error

$$= \frac{AbsoluteError}{TrueValue} x100 \tag{3.11}$$

Relative Error

The formula for Relative error can be written as,

$$RelativeError = \frac{AbsoluteError}{AcceptedValue} \tag{3.12}$$

$$AbsoluteError = TrueValue - ApproximateValue \tag{3.13}$$

The layer thickness estimates for hot mix asphalts was found to be good if the percentage of error is ($\pm$3%). The accuracy on base courses was reasonable, but this was also tied to the inability to physically measure the thickness of bases in older pavements given the mixing of base and subgrade materials at the interface between layers [51].

However; for this research paper percentage of error is not calculated because it require actual thickness from core. Meanwhile relative error has been calculated.

4

RESULT AND DISCUSSION

The proposed noise reduction method described in previous chapter(s) and needs further analysis to evaluate its performance. This chapter introduces signal modeling techniques and evaluating the performance of used prepossessing techniques as well as for the target characterization and thickness estimation.

The relation between attenuation factor to the various parameters of the road pavement has been simulated based on the GPRMax model(See detail Appendix B). The results are as follows.
A simulation result for the case of a flexible pavement where the reflections from the top of the asphalt layer, the basecourse layers interface and the subbase course layers interface are recorded. These reflections depend on the velocity (vi) of the waves propagation, which is governed by the dielectric properties of the materials as a function of the dielectric constant of the material mixture. It is worthwhile to be mentioned that the dielectric properties of asphalt layers depend slightly on the compaction during construction and thus on the pore/void content of the final layer material, as well on the water content.

4.1 MODEL SIMULATION ENVIRONMENT

To model simulation environment by specifying material property form electrical properties perspective (i.e. dielectric values) and selecting proper layer thickness.Taking thickness values from Table 2.4 and the dielectric values are used from Table 2.5. The selected pavement system is three layer and air suspended horn antenna was used.
To simulate each layer: asphalt layer = 12.5cm, basecourse layer = 20cm subbasecourse layer = 27.5cm and also separation between antenna and pavement = 0.5m specified. However, each thickness has been reduced by 50% to reduce simulation time requirement. Finally, the following model has been model for the simulation purposes.

4.1.1 *Incident Signal*

In order to obtain the values of the dielectric constant, we needed both the amplitudes of the surface reflected pulses and the amplitude of the GPR incident signal. However, only the amplitudes of the surface reflected pulses could be ascertained. Therefore, the researcher create a simulation environment to get the incident signal. The GPR was placed on a large metal plate and switched to work. In this case, the amplitude of reflected signal could be considered as the amplitude of the incident signal.

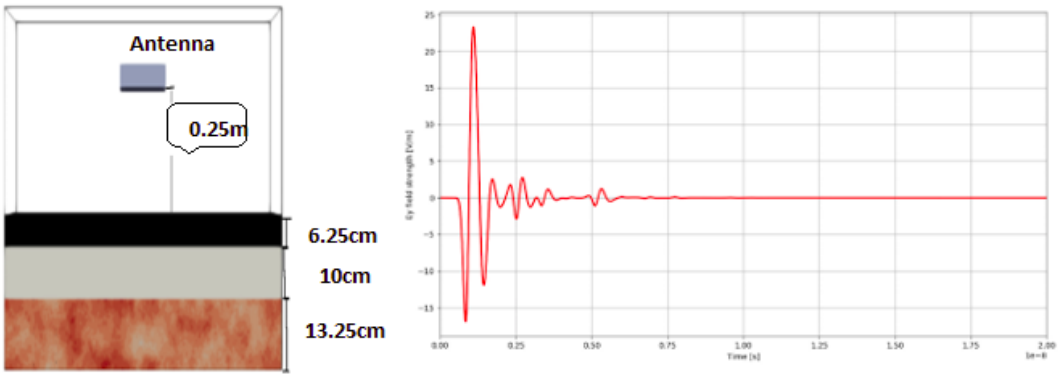

Figure 4.1: Measured Amplitudes and Time Delays for the GPR

Dielectric Value	Amplitude
44.2	Am = 116.2961

Table 4.1: Gold plate reflection amplitude

The intensity of the recorded reflections is proportional to the strength of the contrast in dielectric properties between pavement layers.

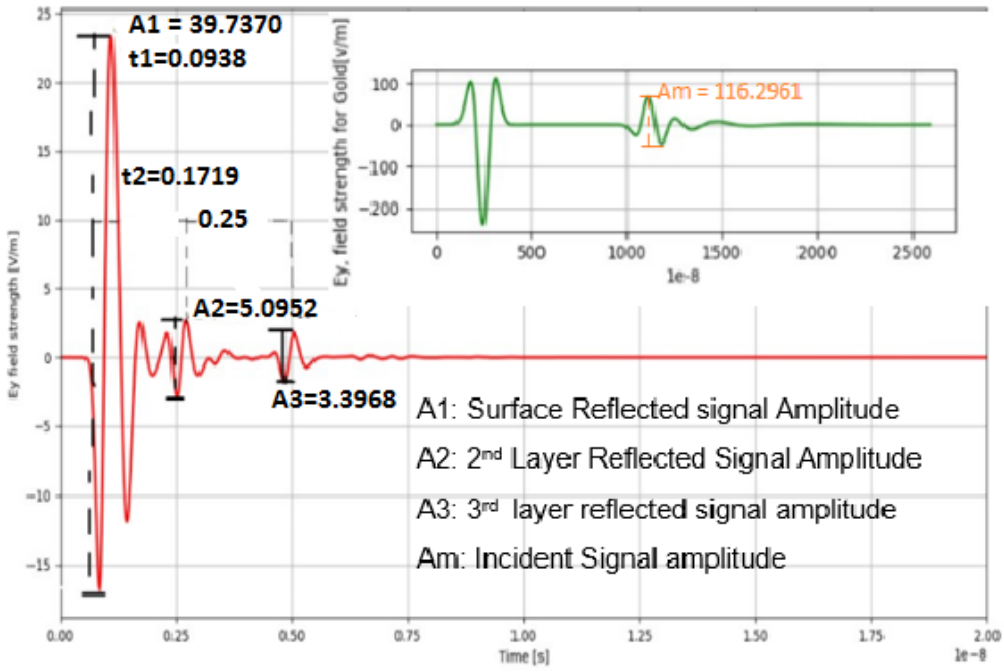

Figure 4.2: GPR trace measured with a 1.5 GHz Horn Antenna

Table 4.1, Figure 4.2 is a repeat of Figure 4.2 showing the measured amplitudes and time delays. To clearly show the peaks an amplitude, the measured values for A1, A2 and A3, are 39.7370, 5.0952 and 3.3968 volts/meter respectively.
The time delay between reflections t1 , t2 and t3 , is 0.0938, 0.1719 and 0.25 nanoseconds.

The amplitude of metal plate reflection Am is shown in Figure 4.2 to be 116.2961 volts/meter. To demonstrate how these equations (described in Chapter 3) are used the HMA will be computed for the individual GPR trace shown in Figure 4.2. Using Equation (3.9) the dielectric constant ε_a of the 1st layer (Asphalt) can be estimated;

Substituting the values that get from the above Figure and Table(Table 4.1 and Figure 4.2) we can calculate the estimated dielectric values of each layer.

- Asphalt Layer:

  $\varepsilon_a = (\frac{1+\frac{Ao}{Am}}{1-\frac{Ao}{Am}})^2 = (\frac{1+(39.7370/116.258)}{1-(39.7370/116.258)})^2$

  ε_a= **4.15219**

- Basecourse Layer:

  $\varepsilon_b = (\frac{1+(\frac{A1}{Am})^2+(\frac{A2}{Am})^2}{1-(\frac{A1}{Am})^2-(\frac{A2}{Am})^2})^2$

  ε_b= **5.0697**

- Subbase Layer:

  $\varepsilon_s = (\frac{1+(\frac{A1}{Am})^2-(\frac{A1A2}{Am})+(\frac{A3}{Am})^2}{1-(\frac{A1}{Am})^2-(\frac{A1A2}{Am})+(\frac{A3}{Am})^2})^2$

  ε_s=**5.4067**

The estimated dielectric values for asphalt is $\varepsilon_a = 4.15219$, estimated dielectic value for base-course is $\varepsilon_b = 5.0697$ and estimated value for sub-base is $\varepsilon_s = 5.4067$.

Exact Dielectric Value	Estimated Dielectric Value	Relative Error %
4	4.15219	3.749%
5	5.0697	1.3748%
2-6 (5)	5.4067	7.522%

Table 4.2: Relative error of dielectric with to exact values

From Table 4.2, the dielectric values of soil varies from 2-6 but for a soil with sand fraction 0.5, clay fraction 0.5, bulk density 2 gram per centimeter cub, sand particle density of 2.66 gram per centimeter cub, and a volumetric water fraction range of 0.001 - 0.25, its dielectric values approximated to 5.

The thickness of the i^{th} layer could be computed according to the following equation.

- First Layer:

  $d_a = \frac{c\triangle t1}{2\sqrt{\varepsilon a}} = \frac{3\times0.0938}{2\times2.0386}$ = **0.069m**

- Second Layer:

  $d_b = \frac{c\triangle t2}{2\sqrt{\varepsilon b}} = \frac{3\times0.1719}{2\times2.2516}$ = **0.1144m**

- Third Layer:

  $d_s = \frac{c\triangle t3}{2\sqrt{\varepsilon s}} = \frac{3\times0.25}{2\times2.325}$ = **0.1613m**

The estimated thickness for asphalt , base-course and sub-base is $d_a = 6.9cm$, $d_b = 11.44cm$ and $d_s = 16.13cm$ respectively.

Exact Thickness Values in cm	Estimated Thickness Value	Relative Error %
6.25	6.9	9.42%
10	11.44	12.58%
13.25	16.13	14.75%

Table 4.3: Relative error of thickness with to exact values

4.2 TEST CASE: LIMESTONE, GRANITE

In this section, Base course layer can be build by different materials depending on the availability of materials.

4.2.1 *Limestone*

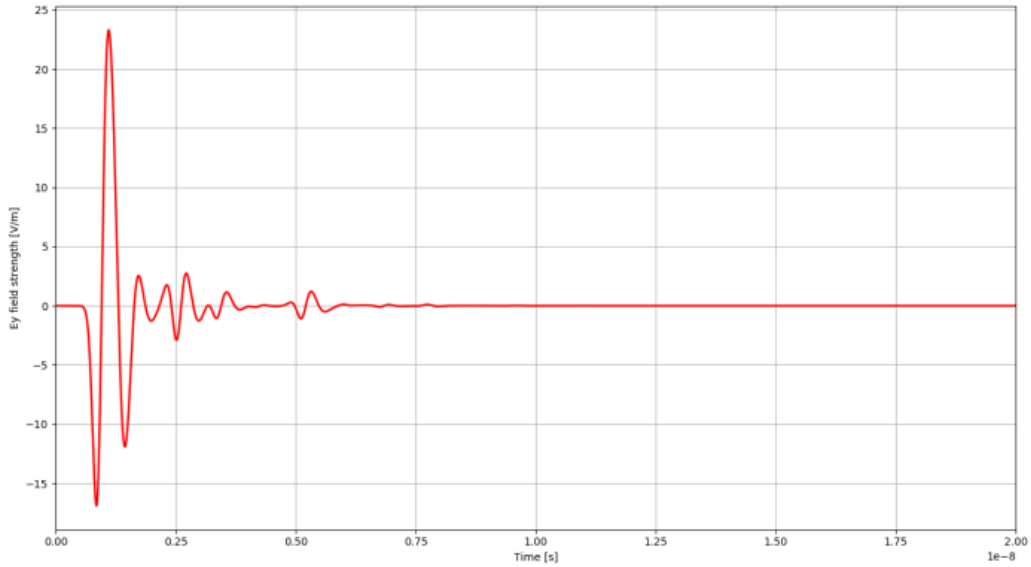

Figure 4.3: Measured Amplitudes and Time Delays by changing basecourse layer to Granite

Figure 4.3 is showing the measured amplitudes and time delays. To clearly show the peaks an amplitude, the measured values for A1, A2 and A3, are 40.1144, 5.5804 and 2.2645 volts/meter respectively.
The time delay between reflections t1 , t2 and t3 , is 0.0938, 0.1875 and 0.2812 nanoseconds.

- Asphalt Layer:

  $\varepsilon_a = (\frac{1+\frac{A_o}{A_m}}{1-\frac{A_o}{A_m}})^2 = (\frac{1+(40.1144/116.258)}{1-(40.1144/116.258)})^2$

  ε_a= **4.2166**

- Basecourse Layer:

  $\varepsilon_b = (\frac{1+(\frac{A1}{A_m})^2+(\frac{A2}{A_m})^2}{1-(\frac{A1}{A_m})^2-(\frac{A2}{A_m})^2})^2$

  ε_b= **5.2445**

- Subbase Layer:

  $\varepsilon_s = (\frac{1+(\frac{A1}{Am})^2-(\frac{A1A2}{Am})+(\frac{A3}{Am})^2}{1-(\frac{A1}{Am})^2-(\frac{A1A2}{Am})+(\frac{A3}{Am})^2})^2$

  ε_s**=5.314**

The estimated dielectric values for asphalt is $\varepsilon_a = 4.266$, estimated dielectic value for base-course is $\varepsilon_b = 5.2445$ and estimated value for sub-base is $\varepsilon_s = 5.3147$.

Exact Dielectric Value	Estimated Dielectric Value	Relative Error %
4	4.2166	5.136%
5	5.2445	4.662%
2-6 (5)	5.3147	5.921%

Table 4.4: Relative error of dielectric with to exact values

The thickness of the i^{th} layer could be computed according to the following equation.

- First Layer:

  $d_a = \frac{c\triangle t1}{2\sqrt{\varepsilon a}} = \frac{3\times0.0938}{2\times2.0534}$ = **0.0685m**

- Second Layer:

  $d_b = \frac{c\triangle t2}{2\sqrt{\varepsilon b}} = \frac{3\times0.1875}{2\times2.2901}$ = **0.1228m**

- Third Layer:

  $d_s = \frac{c\triangle t3}{2\sqrt{\varepsilon s}} = \frac{3\times0.2812}{2\times2.305}$ = **0.183m**

The estimated thickness for asphalt , base-course and sub-base is $d_a = 6.9cm$, $d_b = 11.44cm$ and $d_s = 16.13cm$ respectively.

Exact Thickness Values in cm	Estimated Thickness Value	Relative Error %
6.25	6.085	2.711%
10	12.28	18.56%
13.25	16.13	17.85%

Table 4.5: Relative error of thickness with to exact values

4.2.2 *Granite*

Figure 4.4 is showing the measured amplitudes and time delays. To clearly show the peaks an amplitude, the measured values for A1, A2 and A3, are 39.7424, 5.5804 and 2.2645 volts/meter respectively.
The time delay between reflections t1 , t2 and t3 , is 0.0938, 0.1719 and 0.2422 nanoseconds.

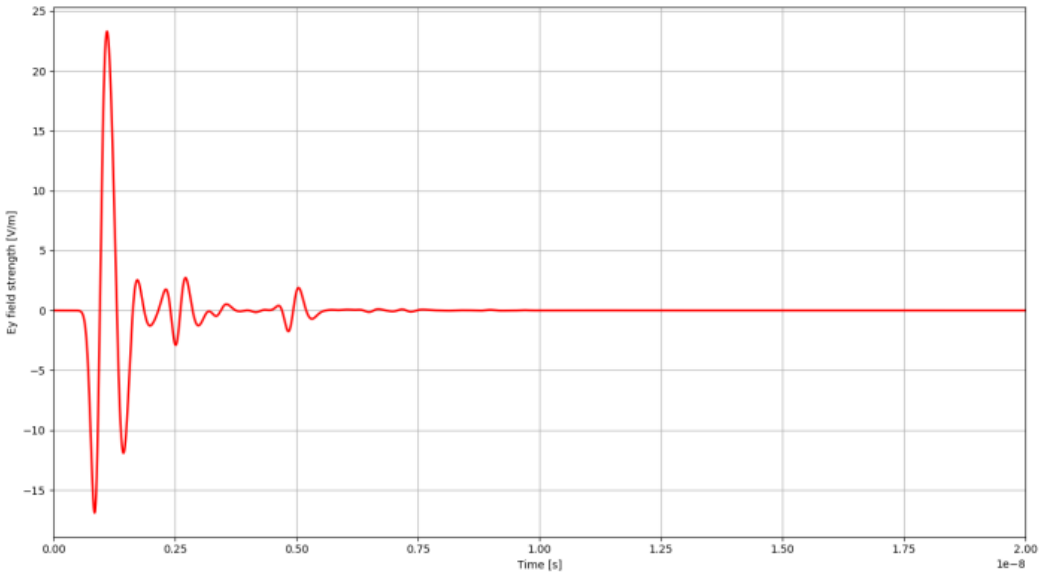

Figure 4.4: Measured Amplitudes and Time Delays by changing basecourse layer to Limestone

- Asphalt Layer:

  $\varepsilon_a = (\frac{1+\frac{Ao}{Am}}{1-\frac{Ao}{Am}})^2 = (\frac{1+(39.7424/116.258)}{1-(39.7424/116.258)})^2$

  ε_a= **4.1912**

- Basecourse Layer:

  $\varepsilon_b = (\frac{1+(\frac{A1}{Am})^2+(\frac{A2}{Am})^2}{1-(\frac{A1}{Am})^2-(\frac{A2}{Am})^2})^2$

  ε_b= **5.2448**

- Subbase Layer:

  $\varepsilon_s = (\frac{1+(\frac{A1}{Am})^2-(\frac{A1A2}{Am})+(\frac{A3}{Am})^2}{1-(\frac{A1}{Am})^2-(\frac{A1A2}{Am})+(\frac{A3}{Am})^2})^2$

  ε_s=**5.314**

The thickness of the i^{th} layer could be computed according to the following equation.

- First Layer:

  $d_a = \frac{c\triangle t1}{2\sqrt{\varepsilon a}} = \frac{3\times0.0938}{2\times2.0534}$ = **0.0685m**

- Second Layer:

  $d_b = \frac{c\triangle t2}{2\sqrt{\varepsilon b}} = \frac{3\times0.1719}{2\times2.2901}$ = **0.1228m**

- Third Layer:

  $d_s = \frac{c\triangle t3}{2\sqrt{\varepsilon s}} = \frac{3\times 0.2422}{2\times 2.3052}$ = **0.183m**

Exact Dielectric Value (Basalt)	Estimated Dielectric Value	Relative Error %
4	4.15219	3.749%
5	5.0697	1.3748%
2-6 (5)	5.4067	7.522%
Exact Dielectric Value(Limestone)	Estimated Dielectric Value	Relative Error
4	4.2166	3.749%
6	6.244	3.91%
2-6 (5)	5.314	5.91%
Exact Dielectric Value(Granite)	Estimated Dielectric Value	Relative Error
4	4.1912	3.749%
5.2	5.228	1.3748%
2-6 (5)	5.314	5.91%

Table 4.6: Dielectric Value with Relative Error with Three Different Base course Material

The above result shows that, they are based on the assumption that the layer materials are non-conductive and homogeneous. This assumption means that the imaginary component of the dielectric constant tends to zero; and the medium does not attenuate the radar signal.
Therefore, all of the energy is either reflected or transmitted and none is lost in heating free water in the layer.

4.3 LAYER SEPARATION

Layer separation indicate that pavement layer composing material distribution across scanning line.

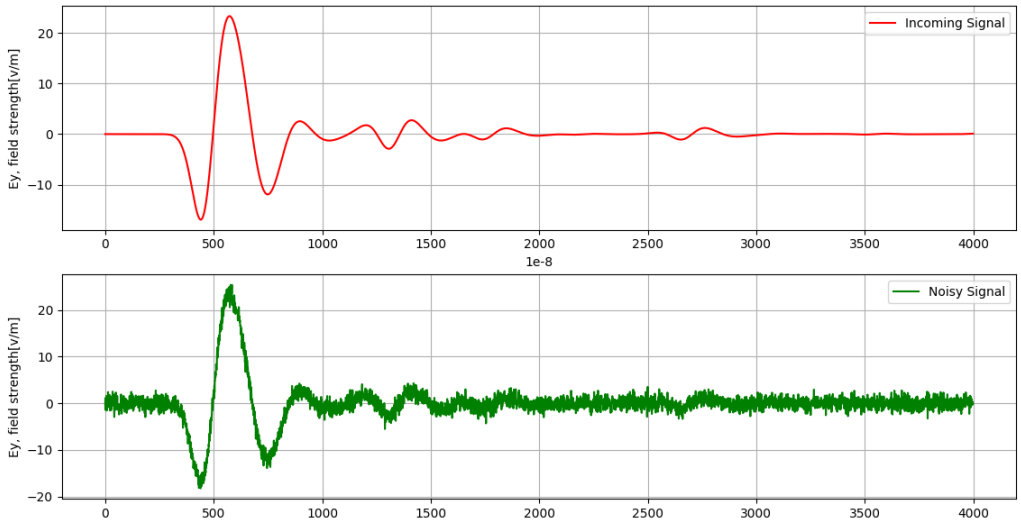

Figure 4.5: AWGN added on Incoming Signal

The Above Figure 4.5, shows that Additive White Gaussian Noise is added on the incoming signal.It indicate that the incoming signal is more corrupted between the time variation t $= 0.0945 - 0.2657$ nanosecond and t $= 2.6785 - 2.92095$ nanosecond. The first figure 4.5 indicate that GPR data plotted with python and the second signal show that AWGN is added on GPR data.

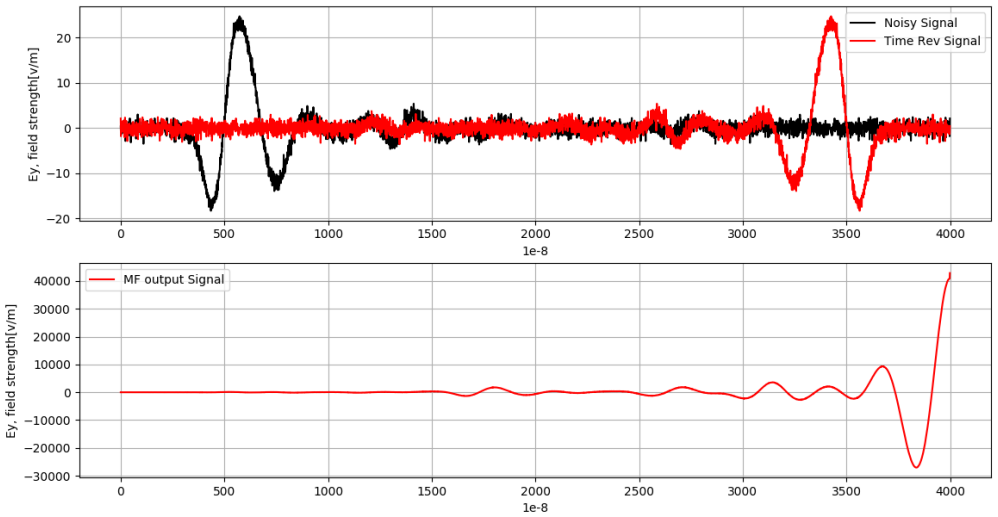

Figure 4.6: Matching Filter Applied on Incoming Signal

From Figure 4.6,considering incoming signal as input, its possible to prepare tem-

plet (i.e. reverse time on incoming signal). After correlation has been done, the amount of noise presented on GPR data was canceled out.

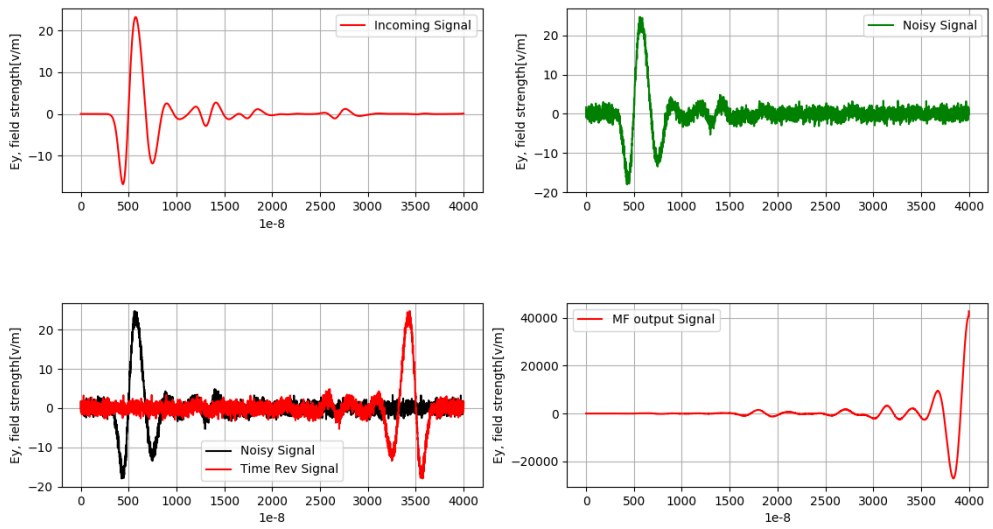

Figure 4.7: Matching Filter Applied on Incoming Signal

Figure 4.8 show that 60 successive incoming signal is merged together and called B scan. The First bold line indicate that asphalt layer and layer has uniform material distribution with fixed layer thickness. The time delay to reach from antenna to asphalt layer is $t_1 = 0.0938 * 10^{-8}$.

The second and third line indicate that Base Course layer (2nd layer) and Sub base

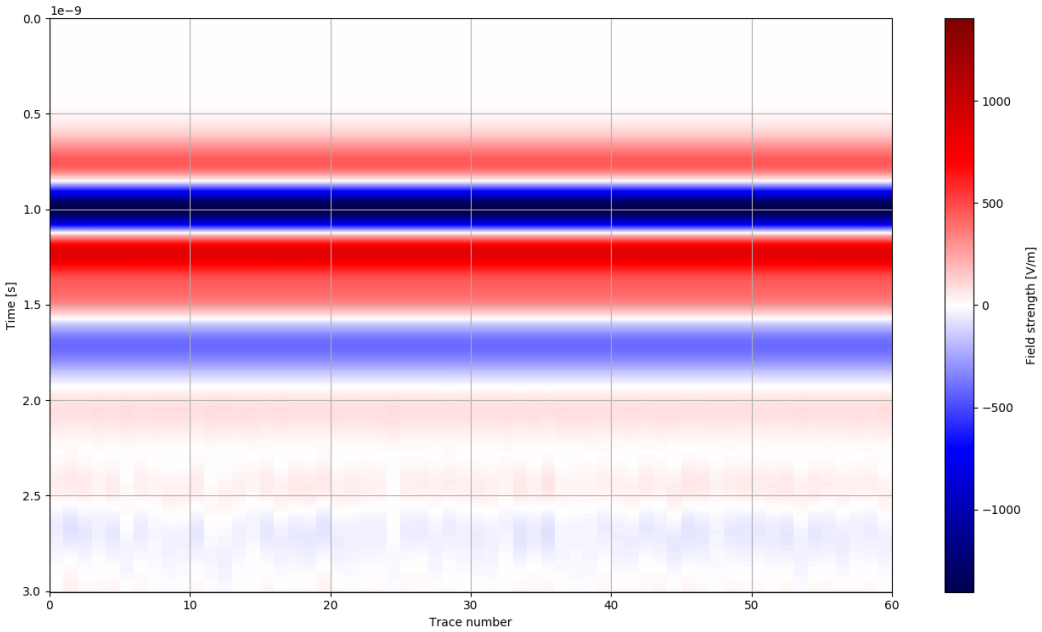

Figure 4.8: Layer Separation Using B scan

course (3rd layer). Each layer has uniform material but the time delay for 2nd layer is $t_2 = 0.2657 * 10^{-8}$ and for the third layer is $t_3 = 0.5157 * 10{-}8$.
It also indicate that constant material distribution and thickness through each layer because each layer consider as uniform material and fixed layer separation.

5

CONCLUSION AND RECOMMENDATION

This chapter will present about the result that have been done on gprMax simulation software and Paraview. Finally, conclusion will be presented and the proposed recommendation will be drawn.

5.1 CONCLUSION

In this thesis, a system for analysis and interpretation of GPR data collected over pavements was developed. Within this system, GPR data is analyzed on a scan by scan basis by passing through successive processing stages. The results obtained from the individual scans A scan are then grouped together B scan to form the different pavement layer interfaces which the layer thicknesses and material types are estimated. The performance of the developed system was evaluated and data is collected from a pavement system .
Based on this research, the following conclusions could be drawn:

- The state of art on thickness and characteristic estimation acquired.
- Test case was introduced to verify the GPR data was acquired from GPRMax simulation software at frequencies (1.5 GHz).
- Data analysis has been done by using matched filter and gained εa , εb and εs 3.749% , 1.374% and 7.522% respectively.
- Percentage of relative error is increase when we go from surface(Asphalt layer) to the bottom(sub grade).

5.2 RECOMMENDATIONS AND FUTURE WORK

In this thesis, A scan signal is processed to estimate layer thickness and to characterize material and B scan signal is processed to indicate layer interface. Matching filter was used to cancel out the effect noise from each layer to estimate dielectric values and thickness. So, Whether asphalt pavements is new or old, the accuracy of layer thickness estimation and material characteristics is very important for engineers. For new asphalts, is essential to ensure that the placed layer(s) meet the designed specifications, as part of quantity control and quality assurance. For the old asphalts pavement, to make appropriate economical rehabilitation decision. Therefore, Ground penetrating radar can be used reliably to non destructively assessment pavement systems and to estimate their layer thicknesses and material characterization.

- The number of layers and thickness section has done randomly for simulation purposes so far, however, it is dependent on number of traffic load and

the researcher will recommend that the some result and percentage of error may varies depending on number of layers and materials.

- In these research it has been considered that the 1st layer has uniform material (i.e, asphalt considered as one material yet for the realistic condition it is not) and also dielectric value considered for dry asphalts. For the 2nd layer, it has been also considered uniform material but the combination of basalt with limestone, basalt with granite, and also limestone with granite is not considered.
- In this study, refraction of signal through pavement layers is not considered in case of a ground-coupled antenna.
- In this study,density and void is not considered which is recommended

BIBLIOGRAPHY

[1] Environmental Impact Assessment. "Federal Democratic Republic of Ethiopia Ethiopian Roads Authority." In: (2012).

[2] Andrea Benedetto and Lara Pajewski. *Civil engineering applications of ground penetrating radar*. Springer, 2015.

[3] IL Al-Qadi and S Lahouar. "Measuring layer thicknesses with GPR–Theory to practice." In: *Construction and building materials* 19.10 (2005), pp. 763–772.

[4] Samer Lahouar. "Development of data analysis algorithms for interpretation of ground penetrating radar data." PhD thesis. Virginia Tech, 2003.

[5] Lawrence B Conyers. *Ground-penetrating radar for archaeology*. AltaMira Press, 2013.

[6] Nurul Bostanudin. "Computational methods for processing ground penetrating radar data." PhD thesis. University of Portsmouth, 2013.

[7] Chi-Chih Chen, L Peters, and Walter D Burnside. "Ground penetration radar target classification via complex natural resonances." In: *Antennas and Propagation Society International Symposium, 1995. AP-S. Digest*. Vol. 3. IEEE. 1995, pp. 1586–1589.

[8] Cédric Le Bastard, Vincent Baltazart, Xavier Dérobert, and Yide Wang. "Support vector regression method applied to thin pavement thickness estimation by GPR." In: *Proceedings of the 14th International Conference on Ground Penetrating Radar*. 2012, pp. 349–353.

[9] Lawrence B Conyers. "Analysis and interpretation of GPR datasets for integrated archaeological mapping." In: *Near Surface Geophysics* 13.6 (2015), pp. 645–651.

[10] Amara Loulizi, Imad L Al-Qadi, and Samer Lahouar. "Optimization of ground-penetrating radar data to predict layer thicknesses in flexible pavements." In: *Journal of transportation engineering* 129.1 (2003), pp. 93–99.

[11] James Clerk Maxwell. *The Scientific Letters and Papers of James Clerk Maxwell: 1846-1862*. Vol. 1. CUP Archive, 1990.

[12] Brian Gee. "André Marie Ampère (1775-1836)." In: *Physics Education* 5.6 (1970), p. 359.

[13] RYAN D Tweney. "Fields of enterprise: On Michael Faraday's thought." In: *Creative people at work: Twelve cognitive case studies* (1989), pp. 91–106.

[14] Karin Reich. "CARL FRIEDRICH GAUSS (1777-1855)." In: *Conferències FME* (1977), p. 75.

[15] Birhaneyesus G/Tsadik. "Time-Frequency Analysis for Landmine Detection Using Impulse Ground Penetration Radar. Master's thesis."

[16] Zehua Dong, Shengbo Ye, Yunze Gao, Guangyou Fang, Xiaojuan Zhang, Zhongjun Xue, and Tao Zhang. "Rapid detection methods for asphalt pavement thicknesses and defects by a vehicle-mounted ground penetrating radar (GPR) system." In: *Sensors* 16.12 (2016), p. 2067.

[17] "Automatic detection of multiple pavementamer Lahouara,b,, Imad L. Al-Qadic." In: *NDT & E International* 41 (2008), pp. 69–81.

[18] Cédric Le Bastard, Vincent Baltazart, Yide Wang, and Joseph Saillard. "Thin-pavement thickness estimation using GPR with high-resolution and super-resolution methods." In: *IEEE Transactions on Geoscience and Remote Sensing* 45.8 (2007), pp. 2511–2519.

[19] Qiang Li, Jie Chen, Xiaojun Liu, and Guangyou Fang. "Non-destructive pavement layer thickness measurement using empirical mode decomposition with GPR." In: *Journal of Electronics (China)* 31.6 (2014), pp. 619–627.

[20] Andreas Loizos and Christina Plati. "Accuracy of pavement thicknesses estimation using different ground penetrating radar analysis approaches." In: *NDT & e International* 40.2 (2007), pp. 147–157.

[21] Raffaele Persico. *Introduction to ground penetrating radar: inverse scattering and data processing*. John Wiley & Sons, 2014.

[22] Alex Martinez and Alan P Brynes. *Modeling dielectric-constant values of geologic materials: An aid to ground-penetrating radar data collection and interpretation*. Vol. 247. Kansas Geological Survey Lawrence, Kansas, 2001.

[23] *gprMax User Guide Release 3.0.0b20*. gprMax User Guide Release 3.0.0b20. 2016.

[24] AP Annan. *Electromagnetic principles of ground penetrating radar*. Vol. 1. chapter, 2009.

[25] Harry M Jol. *Ground penetrating radar theory and applications*. elsevier, 2008.

[26] Gary R Olhoeft. "Applications and frustrations in using ground penetrating radar." In: *IEEE aerospace and electronic systems magazine* 17.2 (2002), pp. 12–20.

[27] Manuel Davy, Christian Doncarli, and G Faye Boudreaux-Bartels. "Improved optimization of time-frequency-based signal classifiers." In: *IEEE Signal processing letters* 8.2 (2001), pp. 52–57.

[28] Ibrahim Elshiekh Ahmed. "Visual inspection and ground penetrating radar investigation of the historical Pulaski County Poor Farm Cemetery." In: (2011).

[29] Kimberly Marie Belli. *Ground penetrating radar bridge deck investigations using computational modeling*. Northeastern University, 2008.

[30] Vasily Klimov. *Nanoplasmonics*. Pan Stanford, 2014.

[31] Michael Grealy. "Resolution of ground-penetrating radar reflections at differing frequencies." In: *Archaeological Prospection* 13.2 (2006), pp. 142–146.

[32] Wolfgang Neubauer, Alois Eder-Hinterleitner, Sirri Seren, and Peter Melichar. "Georadar in the Roman civil town Carnuntum, Austria: an approach for archaeological interpretation of GPR data." In: *Archaeological Prospection* 9.3 (2002), pp. 135–156.

[33] Jürg Leckebusch. "Ground-penetrating radar: a modern three-dimensional prospection method." In: *Archaeological prospection* 10.4 (2003), pp. 213–240.

[34] Khatereh Vaghefi, Renee C Oats, Devin K Harris, Theresa (Tess) M Ahlborn, Colin N Brooks, K Arthur Endsley, Christopher Roussi, Robert Shuchman, Joseph W Burns, and Richard Dobson. "Evaluation of commercially available remote sensors for highway bridge condition assessment." In: *Journal of Bridge Engineering* 17.6 (2011), pp. 886–895.

[35] Max Clark, Michael Gordon, and Mike C Forde. "Issues over high-speed non-invasive monitoring of railway trackbed." In: *NDT & E International* 37.2 (2004), pp. 131–139.

[36] Belén Riveiro and Mercedes Solla. *Non-destructive Techniques for the Evaluation of Structures and Infrastructure*. Vol. 11. CRC Press, 2016.

[37] K Grote, S Hubbard, John Harvey, and Y Rubin. "Evaluation of infiltration in layered pavements using surface GPR reflection techniques." In: *Journal of Applied Geophysics* 57.2 (2005), pp. 129–153.

[38] Bassam Saad, Hani Mitri, and Hormoz Poorooshasb. "Three-dimensional dynamic analysis of flexible conventional pavement foundation." In: *Journal of transportation engineering* 131.6 (2005), pp. 460–469.

[39] David J Daniels. *Ground penetrating radar*. Vol. 1. Iet, 2004.

[40] IL Al-Qadi, S Lahouar, K Jiang, and TE Freeman. "Effects on asphalt aging on hot-mix asphalt dielectric constants." In: *Proc. 83th Annu. Meeting of the Transp. Res. Board*. 2004, pp. 11–15.

[41] JQ Shang and JA Umana. "Dielectric constant and relaxation time of asphalt pavement materials." In: *Journal of infrastructure systems* 5.4 (1999), pp. 135–142.

[42] Tim Bergmann, Johan OA Robertsson, and Klaus Holliger. "Finite-difference modeling of electromagnetic wave propagation in dispersive and attenuating media." In: *Geophysics* 63.3 (1998), pp. 856–867.

[43] Ivo Kusak, Miroslav Lunak, and Zdenek Chobola. "Monitoring of concrete hydration by electrical measurement methods." In: *Procedia Engineering* 151 (2016), pp. 271–276.

[44] Antonios Giannopoulos. "The investigation of transmission-line matrix and finite-difference time-domain methods for the forward problem of ground probing radar." PhD thesis. University of York, 1998.

[45] Kane Yee. "Numerical solution of initial boundary value problems involving Maxwell's equations in isotropic media." In: *IEEE Transactions on antennas and propagation* 14.3 (1966), pp. 302–307.

[46] AJ Devaney. "Geophysical diffraction tomography." In: *IEEE Transactions on Geoscience and Remote Sensing* 1 (1984), pp. 3–13.

[47] Erik M Johansson and Jeffrey E Mast. "Three-dimensional ground-penetrating radar imaging using synthetic aperture time-domain focusing." In: *Advanced Microwave and Millimeter-Wave Detectors*. Vol. 2275. International Society for Optics and Photonics. 1994, pp. 205–215.

[48] Ewout Van Den Berg and Michael P Friedlander. "Probing the Pareto frontier for basis pursuit solutions." In: *SIAM Journal on Scientific Computing* 31.2 (2008), pp. 890–912.

[49] Zehua Dong, Guangyou Fang, Yicai Ji, Yunze Gao, Chao Wu, and Xiaojuan Zhang. "Parameters and structure of lunar regolith in Chang'E-3 landing area from lunar penetrating radar (LPR) data." In: *Icarus* 282 (2017), pp. 40–46.

[50] V Pérez-Gracia, F García García, and I Rodriguez Abad. "GPR evaluation of the damage found in the reinforced concrete base of a block of flats: A case study." In: *NDT & e International* 41.5 (2008), pp. 341–353.

[51] J Wenzlick, T Scullion, and KR Maser. *HIGH ACCURACY PAVEMENT THICKNESS MEASUREMENT USING GROUND PENETRATING RADAR (NONDESTRUCTIVE TESTING FOR QUALITY CONTROL OF NEW PAVEMENT)*. Tech. rep. 1999.

Part I

Appendices

A

SIMULATION SOFTWARE(S)

A.1 vtk! (vtk!): PARAVIEW

ParaView is an open-source, multi-platform data analysis and visualization application. ParaView users can quickly build visualizations to analyze their data using qualitative and quantitative techniques. The data exploration can be done interactively in 3D or programmatically using ParaView's batch processing capabilities.

ParaView was developed to analyze extremely large datasets using distributed memory computing resources. It can be run on supercomputers to analyze datasets of petascale size as well as on laptops for smaller data, has become an integral tool in many national laboratories, universities and industry, and has won several awards related to high performance computation.

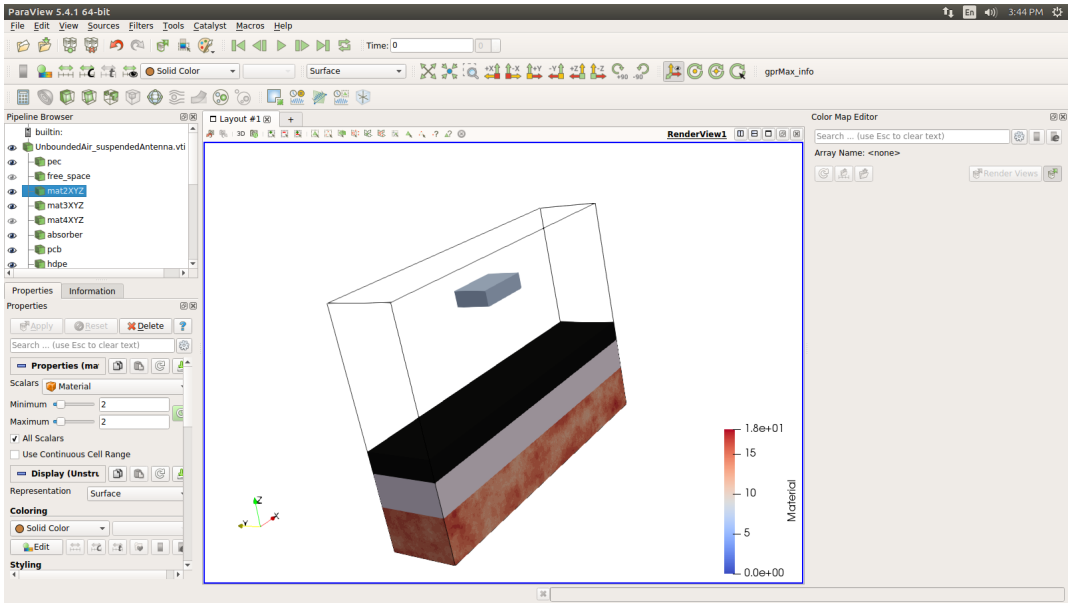

Figure A.1: GPR trace measured with a 1.5 GHz Horn Antenna

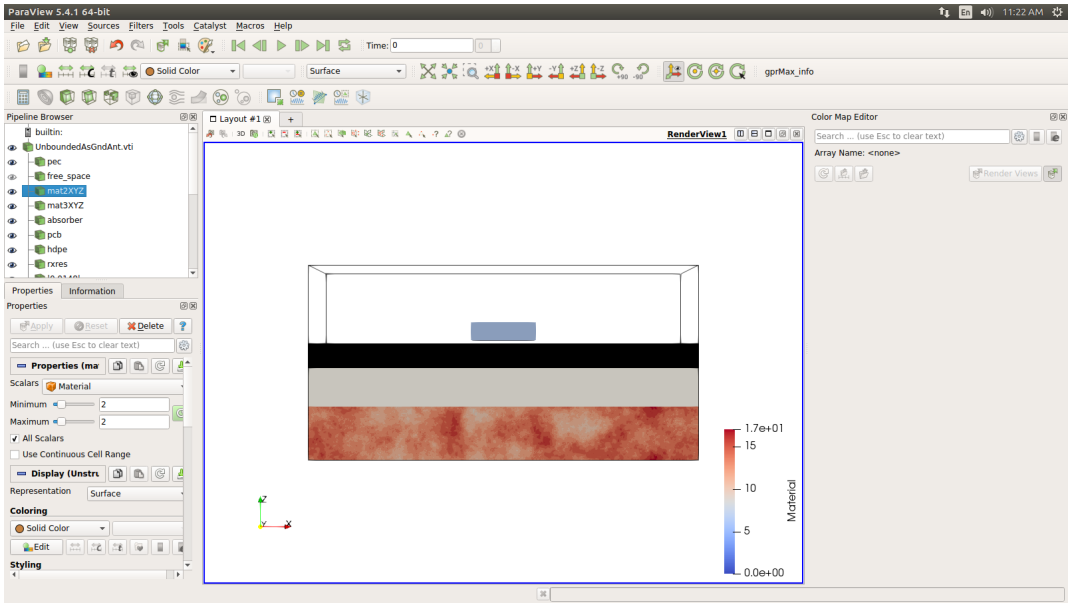

Figure A.2: GPR trace measured with a 1.5 GHz Horn Antenna

B

SIMULATION SOFTWARE

B.1 GPRMAX SOFTWARE

GPRMax is open source software that simulates electromagnetic wave propagation. It uses Yee's algorithm to solve Maxwell's equations in 3D using the Finite-Difference Time-Domain (FDTD) method. The finite difference expressions for the spatial and temporal derivatives are central-difference in nature and second-order accurate.

It is designed for simulating Ground Penetrating Radar (GPR) but can also be used to model electromagnetic wave propagation for many other applications.

GPRMax is command-line-driven software written in Python with performance-critical parts written in Cython. It does not feature a Graphical User Interface (GUI) which allows it to be very flexible and scriptable software that can run in High Performance Computing (HPC) environments, i.e. on supercomputers.
GPRMax can be run on either CPU or GPU. The CPU solver has been parallelised using Open MP which enables it to run on multi-core CPUs. The GPU solver has been developed using the NVIDIA CUDA programming model. GPRMax also features a Messaging Passing Interface (MPI) task farm, which can operate with CPU nodes or multiple GPUs.

GPRMax Software Input
The Input has be saved in.in file formate.
———Addis Ababa University———————
———Addis Ababa Institute of Technology———-
———School of Electrical and Computer Engineering———
———By: Tewodros Mulugeta
———Advisor: Ephrem Teshale(PhD)————
———Co-Advisor: Mekuanent Mulugeta(MSc.)———
———March 12, 2018——
———I am going to build Unbounded Asphalt type with three layer.————
—————-Subbase(Soil)——
—————-Basecoarse(Basalt rock)—-
—————-Asphalt(granite + Bitman)—-
—————-Air———
material: f1 f2 f3 f4 str1
f1 is the relative permittivity, $\varepsilon r =$
f2 is the conductivity (Siemens/metre), $\sigma =$
f3 is the relative permeability, $\mu r =$
f4 is the magnetic loss (Ohms/metre), $\sigma * =$
str1 is an identifier for the material.

NB: *Each layer thickness minimized by half because to minimize computational complexity and to reduce computation time*

title: Asphalt Model Unbounded with Airsuspended Antenna#1
domain: 1 0.208 0.70
#dx − dy − dz : 0.001 0.001 0.001
#$time_window$: 20e-9

——————air = 0.15 - 0.5m (0.25)————————————-

box: 0.0 0.0 0.3 1 0.208 0.55 mat1XYZ
#material: 1 0 1 0 mat1XYZ

————————————Aphalt = 125mm = 0.125m (0.0625)————

#box: 0.0 0.0 0.2375 1.0 0.208 0.3 mat2XYZ
material: 4 0.005 1 0 mat2XYZ

————————————Basecoarse = 200mm = 0.200 (0.1)——

box: 0.0 0.0 0.1375 1.0 0.208 0.2375 mat3XYZ
#material : 6.02771e − 610mat3XYZ

————————————Subbase = 275mm = 0.275m (0.1375)——

soil-peplinski: 0.5 0.5 2.0 2.66 0.001 0.25 soil-properties
fractal-box: 0.000 0.000 0.000 1 0.208 0.1375 1.500 1.00 1.000 1.000 10 soil-properties soil

———-Antenna Parameter——

python:
from user-libs.antennas import antenna-like-GSSI-1500 antenna-like-GSSI-1500(0.5, 0.104, 0.55) #end − python :

—————geometry generating code for vtk——-

```
# geometry-view: 0 0 0 1 0.208 0.70 0.001 0.001 0.001 UnboundedBasaltAir n
```

```
   # By: Tewodros Mulugeta
# Addis Ababa Institute of Technology
# School of Electrical and Computer Engineering
# Advisor: Ephrem Teshale(PhD)
# Co-Advisor: Mr.Mekuanenet Mulugeta (From School of Civil Engineering)
# Title: Asphalt Pavement Thickness Estimation and Material Characterization
# The input file is simulated on gprMax Simulation Software
# The following python code is used to extract Specific Infromation Along different
axis. And also Tell the read about Three Layers of asphalt pavement
# May 2, 2018
# ======================================================================
   import numpy as np
import h5py
import matplotlib.pyplot as plot
import matplotlib.pyplot as plt
from scipy import signal
# Load Data
f = h5py.File('/home/teddy/Desktop/temp/PlotAll/Bscan10.out')

   # Laod Specific (Electric or Magnetic field) along different axis

   d2 = f['/rxs/rx1/Ey']

   # Asign Values for x and y axis
xaxis = np.arange(2.00) \times 0.25e - 8
yaxis = np.arange(2.31) \times 0.4e - 1
# Plot
plot.subplot(321)
plot.plot(d2[0:4000], 'Red')
plot.xlabel('1e-8')
plot.ylabel('Ey, field strength[v/m]')
plt.grid(True)
plot.legend(['Incoming Signal'], loc=0)
# Plot Strait Line and annotation
# Plot

   # plot.show() # ============= Introduce Noise==========# # =============
Generat AWGN Noise==========# import numpy as np
mean = 0
std = 0.01
num-samples = 4000
samples = np.random.normal(mean, std, size = num_samples)
# ============= Filter out Noise Using Matching Filter==========# # ================
Matching Filter====================#
   # Add Generate noise
plot.subplot(322)
```

```
template = d2[0:4000] + samples

   plot.plot(template, 'green')
plot.ylabel('Ey, field strength[v/m]')
plt.grid(True)
plot.legend(['Noisy Signal'], loc=0)
# ============ Introduce Noise==========# # ============ Generat
AWGN Noise==========# import numpy as np
mean = 0
std = 0.01
num_samples = 4000
samples = np.random.normal(mean, std, size = num_samples)
# Apply Time Reverse
plot.subplot(323)
template = d2[0:4000] + samples
fir-coef = template[::-1]
plot.plot(template, 'black')
plot.plot(fir-coef, 'red')
plot.ylabel('Ey, field strength[v/m]')
plot.legend(['Noisy Signal', 'Time Rev Signal'], loc=0)
plot.xlabel('1e-8')
plt.grid(True)
plot.legend(['Noisy Signal', 'Time Rev Signal'], loc=0)
#plot.legend(['Noisy Signal', 'Time Rev Signal'], loc=0)
# Perform Correlation
plot.subplot(324)
det = signal.lfilter(fir_coef, 1, template)
plot.plot(det)
plot.xlabel('1e-8')
plot.ylabel('Ey, field strength[v/m]')
plt.grid(True)
f1 = h5py.File('/home/teddy/Desktop/temp/PlotAll/conductor.out')

   d = f1['/rxs/rx1/Ey']

   xaxis = np.arange(4000)
yaxis = np.arange(2.31)*0.4e-1
plot.subplot(325)
plot.plot(d[0:4000], 'green')
plot.xlabel('1e-8')
plot.ylabel('Ey, field strength for Gold[v/m]')
plt.grid(True)
plot.legend(['Incident Signal'], loc=0)
# Plot Noise Signal
plot.subplot(326)
plot.plot(samples)
```

```
plot.subplots-adjust(hspace=0.6)
plot.show()
```